

Petrology and Geochemistry of an Upper Crustal Pluton: a view into Crustal-scale Magmatism during Arc to Retro-arc Transition

Calvin G. Barnes^{1,*}, W. G. Ernst², Ryan Berry¹ and Tatsuki Tsujimori³

¹Department of Geosciences, Texas Tech University, Lubbock, TX 79409-1053, USA; ²Department of Geological Sciences, Stanford University, Stanford, CA 94305-2115, USA; ³Center for Northeast Asian Studies, Tohoku University, Sendai, Miyagi 980-8576, Japan

*Corresponding author. E-mail: cal.barnes@ttu.edu

Received January 25, 2016; Accepted July 5, 2016

ABSTRACT

The Late Jurassic English Peak plutonic complex was emplaced in an upper crustal retro-arc setting in the central Klamath Mountains province, northern California. Emplacement of the main, central pluton was preceded by intrusion of two satellite bodies: the Uncles Creek pluton crystallized from H₂O-rich quartz dioritic magma with hornblende as the liquidus mafic phase; in contrast, the Heiney Bar pluton is a c. 2.5 km diameter body zoned from gabbro to granodiorite. Al-in-hornblende barometry from these two plutons indicates a stage of magma storage at c. 600–500 MPa. The central English Peak pluton is a c. 15 km diameter body composed of early and late stages. Early stage rocks range from gabbro to tonalite, with variable proportions of augite, orthopyroxene, hornblende and biotite. The early stage lacks discernible zoning and rock types vary at the outcrop scale. This diversity is reflected in bulk-rock compositions, which do not form a compositional array. The late-stage intrusion consists of three concentric units that are zoned from outer, more mafic rocks (quartz diorite, tonalite, quartz monzodiorite) to inner, compositionally evolved rocks (granodiorite and granite). Late-stage samples plot in smooth, typically linear arrays for most major and trace elements. Al-in-hornblende pressures indicate that late-stage hornblende cores grew in a reservoir at c. 400 MPa and that rims grew at the level of final emplacement (c. 250 MPa). The mid-crustal reservoir was the site of late-stage magma evolution, including episodic magma mixing. Oxygen and Sr isotopes indicate initial evolution of English Peak pluton magmas in a deep crustal region of mixing, assimilation, storage, and homogenization (MASH zone), where they were contaminated by metasedimentary rocks. Thus, the English Peak pluton represents a crustal-scale system, with mantle-derived magmas that differentiated near the Moho, storage and crystallization of satellite-pluton magmas in the middle crust (c. 600–500 MPa), development of a large, episodically recharged, magma chamber in the upper middle crust (c. 400 MPa) and final emplacement in the upper crust.

Key words: magmatic systems; Klamath Mountains; geochemistry; arc–retro-arc transition

INTRODUCTION

Physical and petrological models for development of plutonic arc complexes have recently focused on two distinct approaches. The ‘hot zone’ model (e.g. [Annen *et al.*, 2006](#)) envisions that most magma differentiation takes place in the lower crust, with potential transport to upper crustal, sub-volcanic reservoirs where further

magma mixing and fractional crystallization may occur. Alternative models view arc crust as consisting of multiple magma reservoirs or plutons that span most of the crustal column (e.g. [Saleeby *et al.*, 2003](#); [Paterson *et al.*, 2011](#)). In these crustal-scale models, magmas in various stages of solidification may intrude one another, scavenge older magma mushes, mix or mingle, assimilate

host rocks, undergo fractional crystallization and ultimately feed magma resulting from these processes to sub-volcanic reservoirs. Testing these alternative models is generally difficult, particularly in plutonic systems, because few complete sections through arc crust are known (DeBari & Coleman, 1989; Greene *et al.*, 2006; Jagoutz *et al.*, 2009; Otamendi *et al.*, 2009, 2012; Jagoutz, 2010). Moreover, apart from detailed U–Pb dating using high-precision chemical abrasion isotope dilution thermal ionization mass spectrometry methods, the means to identify the characteristics and dimensions of single magma batches in plutons are not well developed.

This study focuses on the Middle to Late Jurassic, upper crustal English Peak plutonic complex (EPC) of the Klamath Mountain province, California, USA. It is one of several Jurassic complexes emplaced in a changing arc setting to a broadly retro-arc setting from Middle Jurassic to Late Jurassic time (Allen & Barnes, 2006). Previous work (Seyfert, 1965; Schmidt, 1994) showed that the EPC was emplaced in stages and that single stages could be identified on a geochemical basis. Here, we summarize the results of previous studies (Seyfert, 1965; Donato *et al.*, 1982; Schmidt, 1994; Ernst, 1998, 1999) along with bulk-rock and mineral geochemical data and a summary of new U–Pb zircon ages. Our goal is to determine the longevity of the complex, placing constraints on the nature of the magma sources and their subsequent geochemical evolution. We build on this database to develop a fuller assessment of the contribution of plutonism to the *P–T*–time history of the crust in the central Klamath Mountains. We conclude that the EPC grew episodically, was formed by amalgamation of several distinct magma batches, and was fed by deeper magma reservoirs that occupied a range of crustal depths. As such, the Klamath Mountains and its plutons provide instructive examples of the formation of the Earth's continental crust.

GEOLOGICAL SETTING

Regional geology

The Klamath Mountain geological province is a terrane collage that consists of four major lithotectonic assemblies. From east to west, these are the Eastern Klamath belt, the Central Metamorphic belt, the Western Paleozoic and Triassic belt (WTrPz), and the Western Jurassic belt (Fig. 1; Irwin, 1960). In general, the tectonostratigraphic terranes that make up each belt are right side up. They are separated by gently east dipping shear zones, most of which are west vergent thrust faults of Paleozoic to Late Jurassic age (Irwin, 1994). Klamath terranes and subterrane contain abundant mafic volcanic and plutonic oceanic rocks as well as continent-derived clastic sedimentary aprons. Thin layers of deep-sea Tethyan chert and limestone cap some of the tectonically dismembered, far-traveled, ophiolites. The terranes were progressively juxtaposed by an inferred component of east-descending

subduction during late Paleozoic to mid-Mesozoic time (Irwin, 1981; Ando *et al.*, 1983; Scherer & Ernst, 2008).

The Western Paleozoic and Triassic belt is host to the EPC and is the largest of the four major lithotectonic belts. It consists of regionally metamorphosed sedimentary, volcanic, ultramafic, and plutonic rocks. In the southern Klamath Mountains, Irwin (1972) divided the WTrPz, from east to west, into the North Fork, Hayfork, and Rattlesnake Creek terranes. Later, the Stuart Fork high-pressure (HP) metamorphic terrane was recognized (Hotz *et al.*, 1977; Goodge, 1989) and the Hayfork terrane was divided into two terranes: Eastern and Western (Wright, 1982; Goodge, 1989). Hacker *et al.* (1993, 1995, and references therein) and Donato (1987, 1989) and Donato *et al.* (1996) demonstrated that many of these WTrPz lithotectonic units extend throughout a broad region of the Klamath Mountains. Figure 1 illustrates the current division of the orogen into mapped tectonostratigraphic terranes (Irwin & Wooden, 1999; Snoke & Barnes, 2006).

A series of broadly calc-alkaline plutons intruded the WTrPz and older belts from Middle Jurassic to Early Cretaceous time (Lanphere *et al.*, 1968; Hotz, 1971; Irwin, 1985; Barnes *et al.*, 1986a, 1992; Irwin & Wooden, 1999; Allen & Barnes, 2006). This magmatic event occurred in a transtensional arc and retro-arc setting, with outboard development of the Josephine ophiolite (Harper & Wright, 1984; Harper *et al.*, 1994) and still further outboard fringing arc magmatism (the Rogue–Chetco arc; Garcia, 1979, 1982). Nevadan and post-Nevadan exhumation exposed a crustal section that extends from upper to lower crustal levels (Coleman *et al.*, 1988; Garlick *et al.*, 2009). As a result, the retro-arc plutons are exposed over a range of crustal levels. One of these, the tilted Wooley Creek batholith (WCB), is adjacent to the EPC to the west and NW (Fig. 1) and exposes at least 12 km of structural relief (Barnes, 1983; Barnes *et al.*, 1986). Accordingly, it is possible to compare the petrochemical evolution of the upper crustal EPC with the WCB.

Local geology

The local bedrock geology is presented in Fig. 2; this is an area that we and previous workers have referred to as the Sawyers Bar area (Irwin, 1960, 1972, 1994; Seyfert, 1965; Ernst, 1987, 1998). Pre-plutonic rock units consist of three tectonically juxtaposed supracrustal units. (1) To the east, the Stuart Fork HP metabasalt–metachert–metagraywacke terrane lies above the low-angle, east-dipping Soap Creek Ridge thrust fault. (2) The medial zone is the North Fork ophiolitic terrane. This consists of St. Clair Creek laminated metacherts and fine-grained quartzofeldspathic argillites interstratified with, and overlain by, two sparsely pillowed, mafic metavolcanic suites—the amygdaloidal, Fe + Ti-rich North Fork mildly alkaline basalts, and the more magnesian Salmon River basaltic–diabasic–gabbroic arc tholeiites. (3) To the west, the eastern Hayfork terrane crops out beneath the high-angle Twin Sisters fault. This terrane consists of a chert–

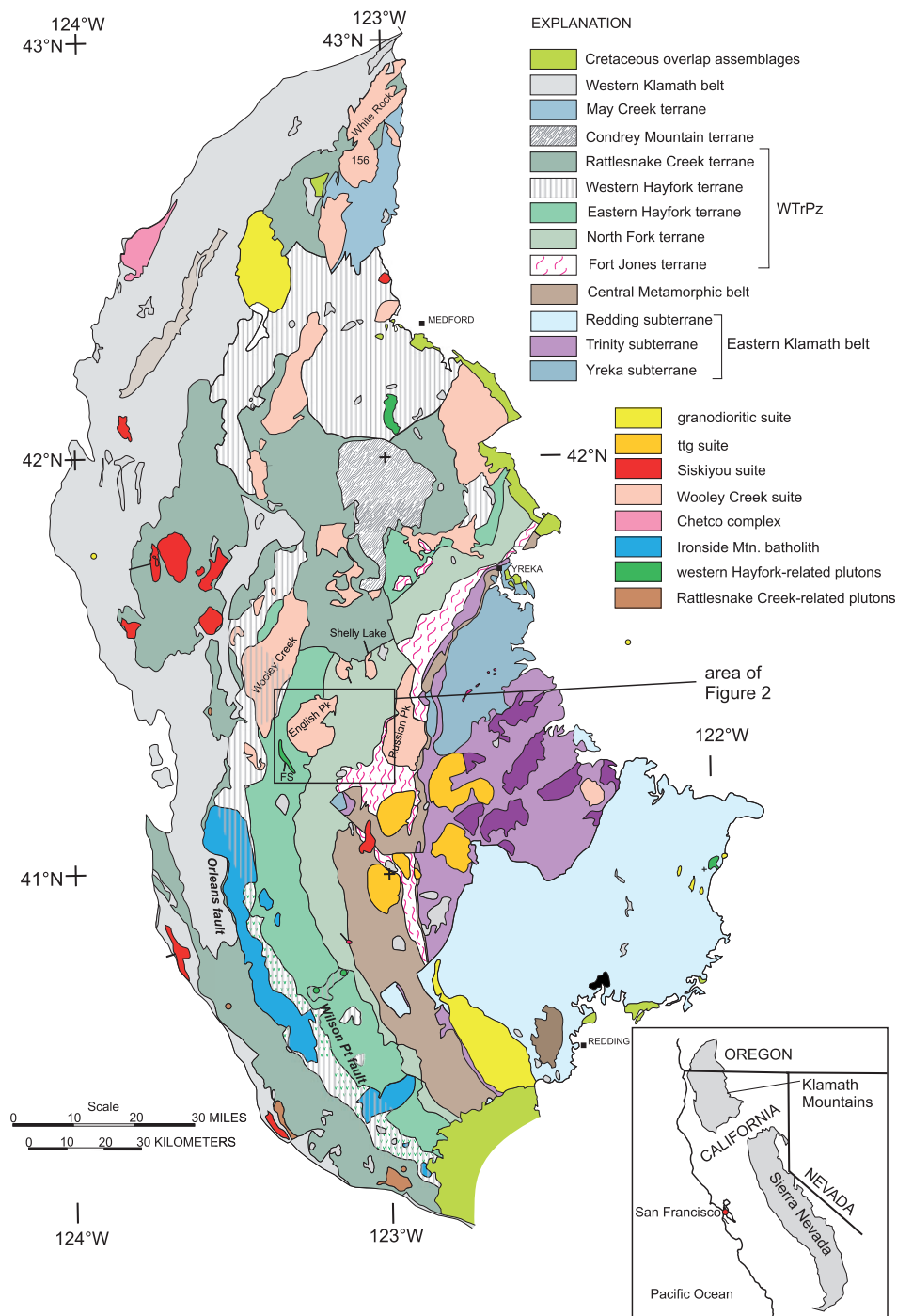


Fig. 1. Lithotectonic divisions and plutonic suites of the Klamath Mountains, after Irwin & Wooden (1999) and Snoke & Barnes (2006). The Fort Jones terrane is equivalent to the Stuart Fork Formation. Plutons are color coded according to age group. In the key, 'ttg suite' refers to Early Cretaceous tonalite–trondhjemite–granodiorite plutons. The granodiorite suite is Early Cretaceous; all other labeled plutonic suites are Jurassic. The inset map shows the location of the Klamath Mountain province and its relationship to the Sierra Nevada province.

argillite ± greywacke mélangé and broken formation with a variety of locally derived and exotic blocks (Wright, 1982; Scherer *et al.*, 2010).

Ernst (1999) advanced the following petrotectonic history for this region. Landward underflow resulted in formation of the high-pressure Stuart Fork blueschist ± eclogite complex, followed by its exhumation

at ~227 Ma (Hotz *et al.*, 1977; Goodge, 1989, 1995). Subsequently, arc tholeiites, alkaline basalts, and distal turbidites of the North Fork and Eastern Hayfork lithotectonic units were deposited in a subsea environment during end-of-Permian(?), Triassic, and earliest Jurassic time (Wright, 1982; Ernst *et al.*, 1991; Mankinen *et al.*, 1996). Submarine eruption and sedimentation continued

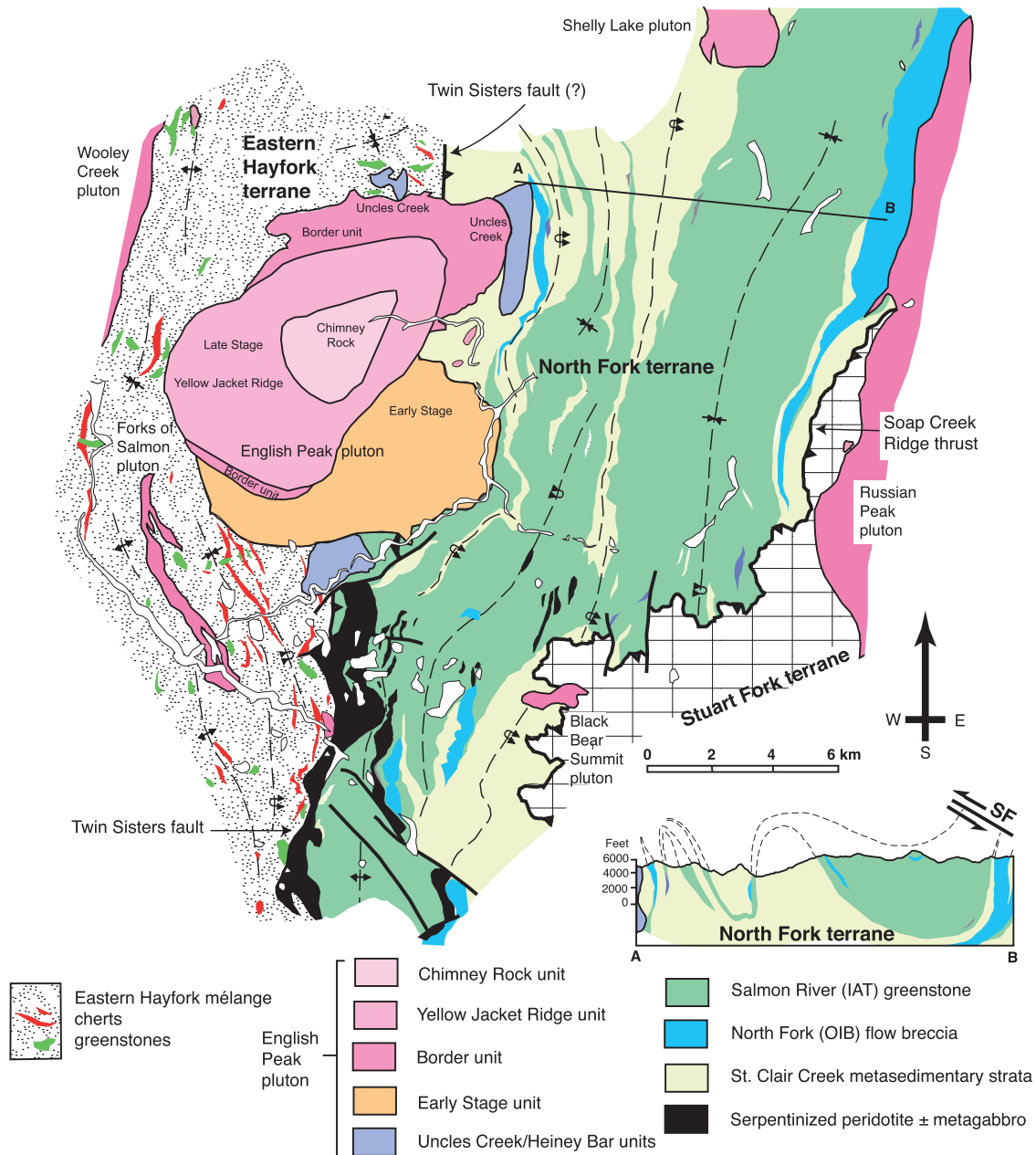


Fig. 2. Geological map of the Sawyers Bar area, after Ernst (1998, 1999). IAT, island arc tholeiite; OIB, ocean island basalt. SF is projected Soap Creek Ridge thrust fault.

in the North Fork arc, and the Eastern Hayfork mélange was disrupted during Early and Middle Jurassic time. By the end of Middle Jurassic time, the yet farther outboard Western Hayfork calc-alkaline arc, along with its basement, the Rattlesnake Creek terrane, had accreted to the Eastern Hayfork terrane (Wright & Wyld, 1994; Barnes *et al.*, 2006). Suturing of the North Fork terrane beneath the Stuart Fork terrane, probably no later than $c. 172 \pm 2$ Ma, resulted in regional folding and isochemical prehnite \pm pumpellyite-facies to biotite-grade greenschist-facies metamorphism under conditions of $300\text{--}425^\circ\text{C}$ and 300 ± 100 MPa.

Mesozoic plutonism in the area began at $c. 174$ Ma (Wright & Fahan, 1988; Allen & Barnes, 2006) and

continued through emplacement of the EPC and adjacent WCB at 159–156 Ma (Coint *et al.*, 2013a, 2013b). Contact metamorphism in the EPC aureole reached maximum temperatures of $\sim 500\text{--}600^\circ\text{C}$ at pressures of 200–300 MPa (Hacker *et al.*, 1992; Ernst, 1999). Fluid exchange in the aureole resulted in local increase in bulk-rock $\delta^{18}\text{O}$ values in North Fork metavolcanic rocks to $>15\%$ (Ernst & Kolodny, 1997).

Geology of the English Peak plutonic complex

The English Peak plutonic complex is the largest intrusive suite in the Sawyers Bar area ($c. 142$ km²). Figure 2 shows the regional geological setting of the EPC. Smaller volume plutons consist of the dike-like,

c. 174 Ma Forks of Salmon pluton (Wright & Fahan, 1988), the 159.1 ± 1.3 Ma Shelly Lake pluton (c. 18 km²; Dorais, 1983; Allen & Barnes, 2006), a suite of micro-diorite dikes emplaced before and during EPC magmatism (Ernst, 1993a), and a suite of alaskitic dikes emplaced after EPC magmatism.

The EPC was recognized by Irwin (1960) as being broadly granitic; in fact, Irwin's (1960) map showed the complex as continuous with the Wooley Creek batholith to the west. Detailed mapping by Seyfert (1965) indicated that these two plutons are, however, separated by c. 4–5 km of metasedimentary rocks of the Eastern Hayfork terrane (Donato *et al.*, 1982; Barnes, 1983). Seyfert (1965) recognized that the EPC consists of three plutonic units. The main body, the English Peak pluton, is nearly circular in outcrop, with a diameter of c. 15 km (Fig. 3). It is flanked by two, smaller, satellite plutons, the Uncles Creek pluton to the NE (c. 4.4 km²) and the Heiney Bar pluton to the south (c. 3.9 km²). The Uncles Creek pluton consists of quartz diorite, tonalite and rare granodiorite, and contains distinctive elongate hornblende crystals. On the basis of similar bulk-rock compositions (see below) and textures, we include the small northern appendage of the EPC (Figs 2 and 3) as part of the Uncles Creek pluton. The Heiney Bar pluton consists of a roughly concentric arrangement of gabbro to granodiorite (Seyfert, 1965).

The main English Peak pluton can be divided into early and late stages (Seyfert, 1965; Schmidt, 1994; this work). The early stage (c. 42 km²) crops out in the southern and southeastern part of the pluton and encompasses gabbro, diorite, quartz diorite, tonalite, quartz monzodiorite, and granodiorite (Fig. 3). The most common mafic assemblage is calcic amphibole (hereafter hornblende) + biotite, but all combinations of hornblende, biotite, augite, and orthopyroxene are present. This variability is clear at the outcrop scale, and as a result, no discernible map-scale zoning pattern in terms of rock types or mafic mineral assemblages was found (Fig. 3). The late stage (c. 91 km²) underlies the central, western, and northern parts of the pluton (Fig. 3) and consists of biotite–hornblende quartz monzodiorite, tonalite, granodiorite, and granite (Figs 3 and 4). Some samples contain relict pyroxene as cores in hornblende; these cores are generally altered to actinolitic amphibole. The late stage of the pluton is zoned, with overall inward increase in the proportions of quartz and K-feldspar, and decrease in color index (CI) from c. 30 to seven (Seyfert, 1965). The late stage was subdivided on the basis of bulk-rock compositions (Schmidt, 1994), and these subdivisions were modified in this work to reflect the expanded dataset. The border unit underlies the northern part of the pluton and forms a kilometer-wide zone along the SW edge of the late stage (Fig. 3); it consists of quartz diorite to granodiorite (Fig. 4). The Yellow Jacket Ridge unit is mainly biotite–hornblende granodiorite; it surrounds the Chimney Rock unit, which is made up primarily of hornblende–biotite granodiorite and granite. The Chimney Rock unit also contains a

number of aplitic dikes, some of which reach 50 m in width. Aplites are sparse elsewhere in the pluton.

Mafic to intermediate composition magmatic enclaves are common in the border and Yellow Jacket Ridge units, both as isolated, rounded to sub-angular masses and as swarms (Schmidt, 1994). The enclaves range from fine- to coarse-grained, with color index from c. 50 to 10. Many contain phenocrysts of plagioclase and hornblende. Double enclaves—heterogeneous enclaves with distinct contacts between two textural types—are common. Fine-grained, mafic, syn-magmatic dikes are widespread but sparse.

Magmatic foliation in rocks of the English Peak pluton is formed by oriented plagioclase, hornblende and magmatic enclaves. Foliation is concentric around the center of the pluton and dips vertically to steeply inwards except along the northern boundary of the Chimney Rock unit, where it dips gently to the south (Seyfert, 1965; this work).

Contacts between EPC plutons and their host rocks are generally sharp (Seyfert, 1965; Donato *et al.*, 1983; Schmidt, 1994; Ernst, 1998), although lit-par-lit injection of the host rocks occurs along the northern contact of the border unit and on the east side of the Uncles Creek pluton, where dikes of Uncles Creek rock type intrude the wall-rocks (Seyfert, 1965; Schmidt, 1994). Xenoliths and screens of the country rocks reach lengths of tens of meters and are common near the northern contact of the English Peak pluton and locally within the Uncles Creek pluton (Seyfert, 1965; Schmidt, 1994). In these areas, some xenoliths are cut and locally disrupted by veins from the host pluton (Gates, 2015). Elsewhere in the complex, xenoliths are sparse, but occur in all of the intrusive units (Seyfert, 1965; Schmidt, 1994; this study).

New U–Pb (zircon) dating by laser ablation inductively coupled plasma mass spectrometry (LA-ICP-MS) (Ernst *et al.*, in preparation) has yielded ages of 172.3 ± 2.0 Ma for the Uncles Creek pluton and 166.9 ± 1.6 Ma for the Heiney Bar pluton. The time interval between emplacement of these two plutons corresponds to a regional thrusting and metamorphic event termed the Siskiyou orogeny (Coleman *et al.*, 1988) that will be considered in greater detail in the Discussion. Ages of the early stage of the English Peak pluton range from 160.4 to 156.6 Ma, including the age of a single sample dated by Allen & Barnes (2006). Ages of the late stage of the English Peak pluton range from 156.3 to 155.3 Ma. The hiatus between emplacement of the satellite plutons and the main English Peak pluton (c. 12 Myr for Uncles Creek and 7 Myr for Heiney Bar) is consistent with sharp intrusive contacts of the latter with the former and with local hydrothermal alteration of the Uncles Creek pluton (Seyfert, 1965; Schmidt, 1995).

PETROGRAPHY

Petrographic descriptions are based on the work of Seyfert (1965), Schmidt (1994) and our new work. Rock

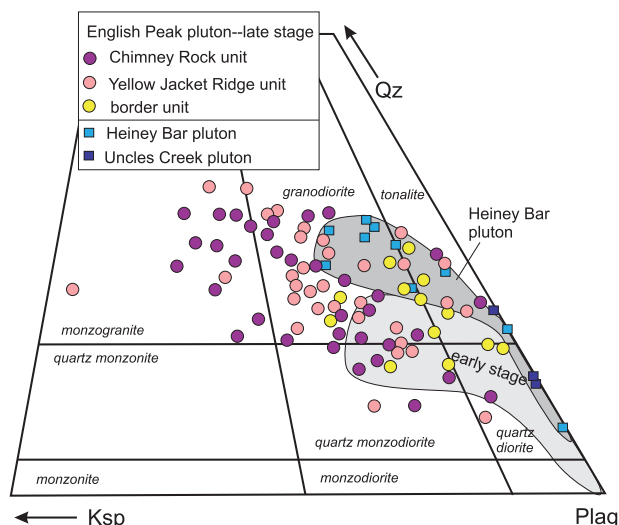


Fig. 4. Representative modal compositions of EPC rocks.

Early stage of the English Peak pluton

Rock types, grain size, and mafic mineral assemblages in the early stage vary greatly (Fig. 4), with CI from 51 to 17 (Schmidt, 1994). In general, these rocks range from medium to coarse grained, are hypidiomorphic granular, and are typified by the presence of augite and orthopyroxene (opx) or their alteration products. Where fresh, the pyroxenes invariably display mutual exsolution, and in some samples augite rims opx. Most commonly, the pyroxenes are rimmed by, or nearly completely replaced by olive-brown hornblende (Fig. 5a). However, some rocks lack hornblende, in which case pyroxenes apparently are in textural equilibrium with biotite (Fig. 5b). Primary pyroxenes commonly are replaced by actinolitic amphibole, which results in cores of secondary (i.e. subsolidus) actinolitic amphibole surrounded by magmatic hornblende. Plagioclase core compositions range from An_{63} to An_{32} with rims from An_{43} to An_{31} (Table 1). K-feldspar is interstitial to sub-poikilitic. Some samples contain bent and/or broken plagioclase tablets. Accessory minerals are apatite, Fe-Ti oxides, and zircon, and locally allanite and titanite. The only occurrences of magmatic titanite are in samples near the southeastern contact of the pluton (Schmidt, 1994). Secondary minerals are blue-green actinolitic amphibole, chlorite, clinozoisite, albite and titanite (after biotite).

Late stage of the English Peak pluton

These rocks are medium- to coarse-grained, hypidiomorphic granular assemblages of plagioclase, hornblende, biotite, quartz, and K-feldspar, and range in composition from quartz diorite to granite. Euhedral to subhedral hornblende is generally prismatic and reaches 6.0 mm in length. Relict pyroxene cores in hornblende are locally present, and are most common in the border unit. With rare exceptions, the pyroxene is replaced by actinolitic amphibole. Zoning is nearly

ubiquitous in hornblende, with pleochroic olive-brown to tan cores that grade abruptly to medium to pale green rims (Fig. 5c and d). In some samples, the core zones are intricately embayed and replaced by green hornblende; such embayments become progressively more prominent inward toward the Chimney Rock unit (Fig. 5d). The green hornblende margins are invariably in contact with sodic plagioclase rims, quartz, or interstitial K-feldspar. Deuteric alteration of hornblende has resulted in local patchy replacement by blue-green actinolitic amphibole. Plagioclase is typically euhedral to subhedral and many grains have weakly zoned, partly resorbed cores and mantles (An_{54-36}) surrounded by oscillatory zoned rims (c. An_{40-19}). Subhedral to euhedral biotite reaches 3.0 mm in diameter and exhibits pale yellow to dark brown pleochroism. In some samples, biotite partially rims and/or replaces hornblende. Quartz is mostly anhedral, but shows crystal faces against K-feldspar. As the abundance of K-feldspar increases inward, its habit varies from interstitial to poikilitic, and in a few of the most evolved Chimney Rock samples, it occurs as subhedral prisms exhibiting Carlsbad twinning. Accessory minerals are apatite, magnetite, zircon, allanite and tourmaline. In addition to actinolitic amphibole, deuteric minerals are chlorite and clinozoisite after hornblende and biotite and white mica after plagioclase.

ANALYTICAL METHODS

Major element mineral compositions were determined by electron microprobe in three laboratories using natural and synthetic standards. Initial work (Schmidt, 1994) was done at Southern Methodist University on a JEOL JXA-733 with analytical conditions of 15 kV accelerating voltage, 20 nA sample current, and 10–20 μm spot diameter. Additional analyses were obtained at the University of Oklahoma and Stanford University. The University of Oklahoma instrument was a Cameca SX50 microprobe equipped with five asynchronous wavelength-dispersive spectrometers and a PGT PRIMS 200 energy-dispersive X-ray analyzer. Operating conditions were 20 kV accelerating voltage, 20 nA sample current and 2 μm spot diameter. The Stanford instrument is a JEOL 8320 microprobe; standard analytical conditions and techniques were used (e.g. Ernst, 1993b). Optical and backscattered electron scanning imagery demonstrated modest zoning in both plagioclase and hornblende, minor along-cleavage heterogeneity among biotite and interlayered subsolidus white mica + chlorite, as well as intimate intergrowths of fine-grained chain-silicate exsolution lamellae in some Ca-rich clinopyroxenes. Nevertheless, where grain sizes exceeded that of the 2–3 μm^3 volume excited by the electron beam, unambiguously single-phase mineral compositions were obtained. In general, core and rim compositions were measured; however, a larger number of analyses were made on samples targeted for trace element analysis (Berry, 2015).

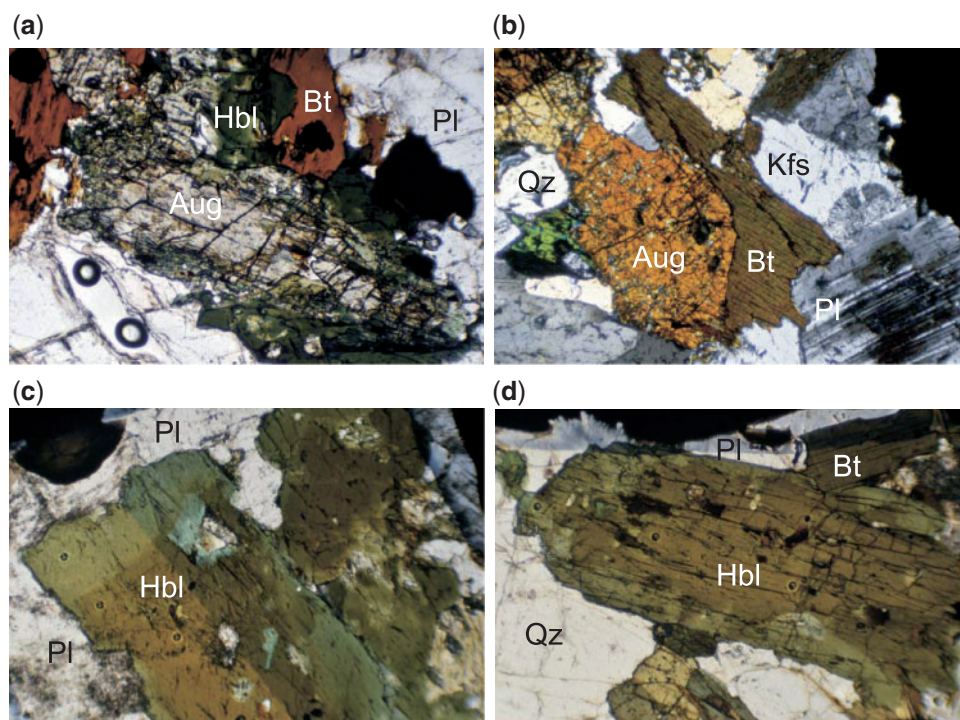


Fig. 5. Photomicrographs. (a) Augite rimmed by hornblende, in turn rimmed by biotite; early stage, English Peak pluton, sample FPE-1488. Plane-polarized light. (b) Augite and biotite in apparent textural equilibrium; early stage, English Peak pluton, sample EP-23. Crossed polars. (c) Hornblende from the border unit, late stage, English Peak pluton. Plane-polarized light. The distinct boundary between olive-brown core and green rim should be noted. Patches of blue-green amphibole are actinolitic. (d) Hornblende from the Chimney Rock unit, late stage, English Peak pluton. Plane-polarized light. Vertical field of view is 1.5 mm for all images.

Cation proportions were calculated assuming that Fe is divalent in the ferromagnesian silicates and white mica, but trivalent in feldspars and clinzoisite. In addition, hydrous phase compositions are reported on an anhydrous basis, assuming their stoichiometric complement of hydroxyl (i.e. a fixed oxygen content). Analyses were rejected when oxide totals and/or cation proportions departed by more than about 3% from the assumed stoichiometric anhydrous values. Accepting these simplifying methods, mineral compositions are presented in Tables 1–4.

Trace element analysis of hornblende was carried out by LA-ICP-MS at Texas Tech University. Samples were ablated using a New Wave UP213 Nd:YAG laser coupled with an Agilent 7500cs ICP-MS system. Laser conditions were 40–55 μm spots, 5 Hz pulse rate, and fluence of 12–14.5 J cm^{-2} . Background (laser off) was counted for *c.* 30 s, followed by *c.* 50 s of analysis. The calibration standard was NIST 612 glass, and USGS glass BHVO-2G was routinely analyzed to assess precision and accuracy. Data were reduced using an Excel spreadsheet (C. M. Allen, personal communication) with internal standardization to CaO, as determined by electron microprobe. Abundances of Ti, P, and Zr were monitored to determine if inclusions of accessory minerals were ablated and, when encountered, the contaminated part of the signal was omitted from the ablation spectrum.

Legacy bulk-rock analyses (Seyfert, 1965; Schmidt, 1992; Ernst, 1998) were performed employing a variety

of methods. Additional samples were analyzed as part of this project, with major oxides and Cr, Cu, Ni, Sr, Ba, V, Zn, and Zr measured by X-ray fluorescence (XRF); the remaining trace elements were measured by LA-ICP-MS on the glass disks used for XRF analysis. The XRF analyses employed an ARL Perform: X 4200 XRF spectrometer, equipped with LiF200, LiF220, AX03, PET, and Ge111 crystals, operating at 30–60 kV, 60–120 mA, and count times of 8–40 s. US Geological Survey standards BHVO-1, GSP-1, STM-1, PCC-1, RGM-1, and AGV-1 were used for calibration. The LA-ICP-MS analyses of the glass disks were acquired on the same instrumental set-up used for trace element analysis of minerals, with laser operation conditions of 40 μm spot, 5 Hz pulse rate, and fluence of 12–14.5 J cm^{-2} . Five spots were analyzed on each disk and these analyses were averaged. Calibration used NIST 612 glass.

RESULTS

Mineral compositions

Feldspars

Plagioclase compositions are discussed in the Petrography section and reported in Table 1. Untwinned K-feldspar, generally orthoclase, occurs in most samples of the EPC. Compositions range from Or_{86} to Or_{98} , averaging $\text{Or}_{93 \pm 05}$ (Table 1), with negligible An contents. Analyzed orthoclase grains from quartz diorites and granodiorites are chemically

Table 1. Representative feldspar compositions

Sample: Spot:	Heiney Bar pluton			English Peak pluton				
	RBEP-005 pl rim	RBEP-005 pl core	RBEP-005 Ksp	Early stage		Late stage		
				FPE-1188 pl core	FPE-1188 pl rim	RBEP-021 Ksp	Border unit	
							RBEP-021 pl core	RBEP-021 pl rim
<i>Oxides (wt %)</i>								
SiO ₂	60.58	56.48	63.87	59.41	60.16	63.70	55.21	55.24
TiO ₂	b.d.l.	b.d.l.	b.d.l.	0.03	b.d.l.	0.03	0.02	0.02
Al ₂ O ₃	24.37	27.24	18.59	25.74	24.72	19.02	27.87	28.11
FeO	0.09	0.10	0.04	0.17	0.17	0.06	0.08	0.12
CaO	6.30	9.57	b.d.l.	7.25	6.33	0.03	10.13	10.05
Na ₂ O	8.14	6.11	0.97	7.23	7.76	1.07	5.58	6.08
K ₂ O	0.18	0.15	16.55	0.25	0.12	15.59	0.16	0.10
Total	99.65	99.65	100.02	100.07	99.25	99.50	99.04	99.71
<i>Cations per 8 oxygens</i>								
Si	2.706	2.546	2.969	2.649	2.696	2.961	2.508	2.497
Ti	b.d.l.	b.d.l.	b.d.l.	0.001	b.d.l.	0.001	0.001	0.001
Al	1.283	1.447	1.018	1.353	1.306	1.042	1.492	1.497
Fe	0.003	0.004	0.001	0.006	0.007	0.002	0.003	0.004
Ca	0.301	0.462	b.d.l.	0.346	0.304	0.001	0.493	0.486
Na	0.705	0.534	0.088	0.625	0.674	0.097	0.491	0.533
K	0.010	0.009	0.981	0.014	0.007	0.925	0.009	0.006
Sum	5.009	5.002	5.057	4.994	4.992	5.028	4.996	5.023

Sample: Spot:	English Peak pluton								
	Late stage								
	Border unit		Yellow Jacket Ridge unit				Chimney Rock unit		
	EP-121 pl rim	EP-121 pl core	RBEP-023 pl core	RBEP-023 pl rim	RBEP-023 Ksp	EP-176B pl core	EP-176B pl rim	EP-169 pl core	EP-169 pl rim
<i>Oxides (wt %)</i>									
SiO ₂	55.53	55.04	61.23	62.90	63.32	56.84	59.61	56.09	66.42
TiO ₂	b.d.l.	0.01	0.02	0.01	0.01	b.d.l.	b.d.l.	b.d.l.	b.d.l.
Al ₂ O ₃	28.31	28.35	23.77	22.74	18.44	27.75	25.59	28.26	21.32
FeO	0.12	0.14	0.07	b.d.l.	b.d.l.	0.03	0.05	0.08	0.04
CaO	10.24	10.50	5.12	4.11	b.d.l.	9.11	6.83	9.79	1.46
Na ₂ O	5.67	5.46	8.82	9.49	0.39	6.14	7.51	5.79	10.67
K ₂ O	0.20	0.16	0.25	0.14	17.31	0.13	0.11	0.19	0.10
Total	100.07	99.66	99.28	99.39	99.47	100.00	99.70	100.20	100.01
<i>Cations per 8 oxygens</i>									
Si	2.499	2.488	2.740	2.800	2.968	2.547	2.662	2.515	2.911
Ti	0.000	0.000	0.001	0.000	0.000	b.d.l.	b.d.l.	b.d.l.	b.d.l.
Al	1.501	1.510	1.254	1.193	1.019	1.465	1.347	1.493	1.101
Fe	0.004	0.005	0.003	b.d.l.	b.d.l.	0.001	0.002	0.003	0.001
Ca	0.493	0.509	0.246	0.196	b.d.l.	0.437	0.327	0.470	0.069
Na	0.495	0.479	0.765	0.819	0.036	0.533	0.650	0.503	0.907
K	0.012	0.009	0.014	0.008	1.035	0.007	0.006	0.011	0.006
Sum	5.004	5.001	5.022	5.017	5.058	4.991	4.993	4.996	4.995

pl, plagioclase; Ksp, K-feldspar; b.d.l., below detection limit.

indistinguishable. Because analyzed crystals lie along the low-temperature part of the K-rich limb of the Ab–Or solvus, extensive subsolidus re-equilibration is indicated.

Pyroxenes

Augite and opx, or their reaction and alteration products, are nearly ubiquitous in the early stage of the English Peak pluton; clinopyroxene is generally better preserved than opx. Clinopyroxene in most samples is augite, but ranges toward diopside, with compositions

in the range $Wo_{49-40}En_{42-36}Fs_{20-13}$ (Fig. 6; Table 2). The clinopyroxene is characterized by low TiO₂ (<0.7 wt %) and Al₂O₃ (mostly <2.0 wt %). Orthopyroxene ($Wo_{1.5-4.1}En_{58-53}Fs_{45-40}$; Fig. 6) is Fe-rich enstatite.

Ca-clinoamphibole

Amphibole in the EPC may be broadly classified as hornblende trending towards actinolite (Fig. 7a; Table 3; classification of Leake *et al.*, 1997). Most of the data plot in the magnesianhornblende field, with a few analyses in the ferrohornblende field. We classify amphibole with

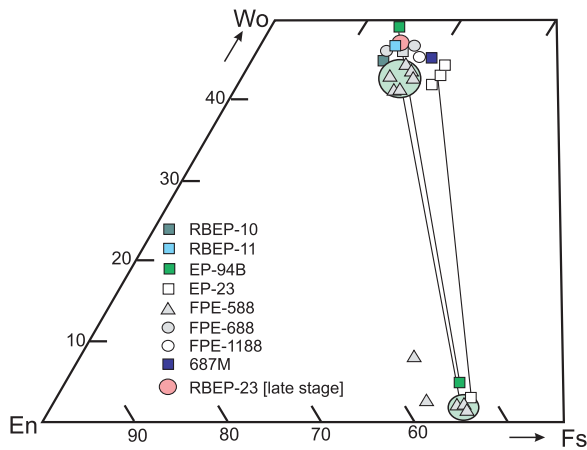


Fig. 6. Pyroxene compositions. All samples are from the early stage of the English Peak pluton.

>7.5 Si per formula unit (p.f.u.) as actinolite, which tends to have slightly higher Mg/(Mg + Fe) than hornblende. In addition, for a given Si content, actinolite in early stage samples tends to be slightly more magnesian than in late-stage samples.

Hornblende in the Uncles Creek and Heiney Bar plutons is distinct in having lower Na contents, and generally lower Ti contents than hornblende from the English Peak pluton (Fig. 7b and c). In addition, hornblende from the Uncles Creek pluton is distinct in having higher Mg/(Mg + Fe) and Al, and lower K (Fig. 7d). Among hornblende from the late-stage English Peak units, distinct populations can be identified on the basis of Ti content (Fig. 7b): olive-brown cores have >0.15 Ti p.f.u., whereas green rims and embayed zones have 0.15–0.05 Ti p.f.u. Actinolitic blue-green amphibole generally has <0.05 Ti p.f.u. The core-rim distinctions evident from Ti abundances are also evident in trace element data. For example, olive-brown cores have higher contents of Zr and Sr (Fig. 7e and f) and total REE (not shown) compared with green rims and embayed zones. The core-rim transition occurs at ~55 ppm Zr and 45 ppm Sr (Fig. 7e and f).

Biotite

Compositional variation in biotite is indistinct within a single specimen. Biotite in the Heiney Bar pluton has lower Mg/Fe than biotite from samples of the English Peak pluton (Fig. 8; Table 4). Within the English Peak pluton, proportions of Ti, Na, and K lack systematic correlations with each other as well as with Si contents and Mg/Fe ratios, and compositional ranges within samples overlap. Although we attempted to avoid interlayered, cryptocrystalline chlorite during microprobe analysis, the analyzed igneous biotite probably was modified to a variable extent by deuteric reactions attending post-magmatic cooling.

Clinozoisite, chlorite, and white mica

Clinozoisite is nearly the stoichiometric Al-end member. Similarly, the analyzed white mica closely approximates

end-member muscovite, and thus is probably a near-solidus phase, rather than the very fine-grained deuteric sericite clusters present in the cores of some plagioclase laths (Supplementary Data Table 1; supplementary data are available for downloading at <http://www.petrology.oxfordjournals.org>). Analyzed chlorites are intermediate Fe–Mg solid solutions and represent late-stage replacements of mafic igneous phases.

Igneous versus deuteric phase compositions

Magmatic crystallization of the EPC was followed by widespread, locally intense deuteric and/or hydrothermal alteration, particularly in the two satellite plutons. Thus, textural relationships and microprobe analyses reflect an incompletely equilibrated recrystallization sequence, making thermobarometric computation of magmatic history problematic. Nevertheless, many samples preserve intricate zoning patterns in hornblende and plagioclase; this feature indicates that the magmatic paragenesis in these samples can be closely approximated.

Major and trace element compositions

Considered together, EPC rocks can be classified as calc-alkalic and magnesian (Frost *et al.*, 2001); all but the most SiO₂-rich samples are metaluminous, and in the few peraluminous samples, the alumina saturation index is less than 1.10. Samples from the Uncles Creek pluton have SiO₂ contents between 50 and 60 wt % (Table 5). These rocks display a wide range of Al₂O₃ contents, and have low abundances of TiO₂, P₂O₅, Rb, and Y compared with samples from the early stage of the English Peak pluton with similar SiO₂ contents (Figs 9 and 10). Samples from the Heiney Bar pluton are bimodal in terms of SiO₂ content, with values <55 wt % and >65 wt %. Compared with the main English Peak pluton, Heiney Bar samples tend to have lower Mg/(Mg + Fe_t) (where Fe_t represents total Fe content) and TiO₂, with widely variably abundances of Al₂O₃ (Fig. 9).

Samples from the early stage of the English Peak pluton range in SiO₂ from ~48 to 61 wt % (Table 5). These rocks vary widely in Mg/(Mg + Fe_t), Al₂O₃, Sc, Y, and Zr (Figs 9 and 10), with no evident correlation with SiO₂. Only among late-stage samples of the English Peak pluton do most elements correlate regularly with SiO₂. Bulk compositions of late-stage rocks increase in SiO₂, total alkalis, and Rb from the border group inward and decrease in Mg/(Mg + Fe_t), Al₂O₃, TiO₂, P₂O₅, Sc, Zr, and Y (Figs 9 and 10). Most of these elements form relatively narrow compositional arrays in plots versus SiO₂. However, Ba abundances are widely scattered and are not correlated with SiO₂ contents (Fig. 10f). In addition, Zr contents in two rocks from the border unit are significantly higher than in other late-stage samples (Fig. 10e).

Rare earth element (REE) abundances in samples from the Uncles Creek and Heiney Bar plutons are lower than those in samples from the early stage of the English Peak pluton (Fig. 11a). Mafic samples from

Table 2. Representative pyroxene analyses

Sample: Analysis:	Augite												
	English Peak pluton, early stage												
	RBEP-010 cpx-5	RBEP-011 cpx-119	RBEP-013 cpx-127	687M cpx-205	FPE-1188 px8-1	FPE-588 px11-3	FPE-588 px1-1	FPE-588 px6-2	FPE-588 px13-2	FPE-688 px12-2	FPE-688 px5-1	EP-23	EP-94B
<i>Oxides (wt %)</i>													
SiO ₂	53.59	53.12	52.16	52.20	52.47	51.59	50.95	51.86	50.67	52.44	52.54	52.39	51.51
TiO ₂	0.28	0.26	0.46	0.14	0.08	0.23	0.64	0.45	0.69	0.29	0.16	0.15	0.26
Al ₂ O ₃	2.23	1.50	1.55	0.95	0.76	1.06	2.41	1.85	2.25	1.35	0.76	1.13	0.94
Cr ₂ O ₃	0.17	0.41	0.01	0.01	n.d.	n.d.	n.d.	n.d.	n.d.	n.d.	n.d.	n.d.	n.d.
MgO	13.63	14.73	13.14	12.06	12.80	13.36	13.18	13.95	13.19	14.08	12.91	12.45	12.64
FeO	8.18	7.10	9.87	11.26	11.14	11.38	10.68	10.38	11.33	8.76	9.74	12.31	11.02
MnO	0.31	0.28	0.45	0.66	0.49	0.43	0.26	0.26	0.29	0.36	0.53	0.50	0.39
CaO	21.30	22.53	22.05	21.65	22.16	21.51	21.17	20.88	20.94	21.64	22.74	20.65	23.22
Na ₂ O	0.44	0.34	0.34	0.36	0.39	0.28	0.37	0.30	0.33	0.35	0.38	0.32	0.31
K ₂ O	0.10	b.d.l.	b.d.l.	b.d.l.	b.d.l.	b.d.l.	b.d.l.	b.d.l.	b.d.l.	b.d.l.	b.d.l.	n.d.	n.d.
Total	100.21	100.26	100.00	99.27	100.32	99.83	99.68	99.98	99.75	99.30	99.76	99.90	100.29
<i>Pyroxene formula calculated according to Droop (1987)</i>													
Si	1.989	1.961	1.953	1.984	1.966	1.939	1.914	1.938	1.907	1.965	1.973	1.980	1.931
Ti	0.008	0.007	0.013	0.004	0.002	0.007	0.018	0.013	0.020	0.008	0.005	0.004	0.007
Al	0.097	0.065	0.069	0.042	0.034	0.047	0.107	0.081	0.100	0.060	0.034	0.050	0.042
Cr	0.005	0.012	0.000	0.000	n.d.	n.d.	n.d.	n.d.	n.d.	n.d.	n.d.	n.d.	n.d.
Fe ³⁺	0.000	0.011	0.024	0.009	0.059	0.081	0.056	0.039	0.072	0.020	0.039	0.005	0.104
Fe ²⁺	0.254	0.208	0.285	0.349	0.290	0.276	0.280	0.286	0.285	0.255	0.267	0.384	0.242
Mn	0.010	0.009	0.014	0.021	0.016	0.014	0.008	0.008	0.009	0.011	0.017	0.016	0.012
Mg	0.754	0.811	0.733	0.683	0.715	0.749	0.738	0.777	0.740	0.787	0.723	0.701	0.707
Ca	0.847	0.891	0.884	0.881	0.890	0.866	0.852	0.836	0.844	0.869	0.915	0.836	0.933
Na	0.032	0.025	0.025	0.027	0.028	0.020	0.027	0.022	0.024	0.025	0.028	0.023	0.023
K	0.005	b.d.l.	b.d.l.	b.d.l.	b.d.l.	b.d.l.	b.d.l.	b.d.l.	b.d.l.	b.d.l.	b.d.l.	n.d.	n.d.
Total	4.000	4.000	4.000	4.000	4.000	4.000	4.000	4.000	4.000	4.000	4.000	4.000	4.000
Analyst	1	1	1	1	2	2	2	2	2	2	2	3	3

Sample: Analysis:	Augite						Orthopyroxene					
	Mafic dikes			Mafic magmatic enclaves			English Peak pluton, early stage				Mafic dikes	
	EP-50	EP-50	EP-56B	EP-12	EP-12	EP-74B	EP-23	EP-94B	FPE-588 px5-4	FPE-588 px9-1	EP-50	EP-56B
<i>Oxides (wt %)</i>												
SiO ₂	52.07	51.41	50.59	53.49	52.58	52.44	51.97	51.86	51.50	51.04	52.63	51.15
TiO ₂	0.51	0.88	0.49	0.23	0.21	0.28	0.23	0.26	0.43	0.20	0.30	0.19
Al ₂ O ₃	2.25	3.52	2.23	1.35	1.05	1.26	0.83	0.69	1.26	0.79	1.45	0.59
Cr ₂ O ₃	n.d.	n.d.	n.d.	n.d.	n.d.	n.d.	n.d.	n.d.	n.d.	n.d.	n.d.	n.d.
MgO	14.68	15.22	12.95	13.68	13.04	12.82	18.39	18.56	19.68	17.62	21.92	17.42
FeO	11.27	10.17	12.68	10.59	11.12	9.50	27.59	27.17	23.15	23.83	22.22	29.14
MnO	0.34	0.25	0.38	0.49	0.62	0.44	0.70	0.82	0.49	0.64	0.44	0.93
CaO	18.59	17.90	20.54	19.03	21.07	23.39	1.42	1.61	3.62	6.43	1.64	0.99
Na ₂ O	0.33	0.67	0.36	0.38	0.47	0.38	0.02	0.05	0.05	0.03	0.04	0.01
K ₂ O	n.d.	n.d.	n.d.	n.d.	n.d.	n.d.	n.d.	n.d.	b.d.l.	b.d.l.	n.d.	n.d.
Total	100.04	100.02	100.22	99.24	100.16	100.51	101.15	101.02	100.24	100.59	100.64	100.42
<i>Pyroxene formula calculated according to Droop (1987)</i>												
Si	1.942	1.902	1.900	2.018	1.971	1.954	1.966	1.961	1.935	1.929	1.949	1.964
Ti	0.014	0.024	0.014	0.007	0.006	0.008	0.007	0.007	0.012	0.006	0.008	0.005
Al	0.099	0.154	0.099	0.060	0.046	0.055	0.037	0.031	0.056	0.035	0.063	0.027
Cr	n.d.	n.d.	n.d.	n.d.	n.d.	n.d.	n.d.	n.d.	n.d.	n.d.	n.d.	n.d.
Fe ³⁺	0.013	0.041	0.101	0.000	0.035	0.049	0.020	0.036	0.055	0.098	0.026	0.036
Fe ²⁺	0.339	0.274	0.298	0.334	0.314	0.247	0.852	0.823	0.672	0.656	0.663	0.900
Mn	0.011	0.008	0.012	0.016	0.020	0.014	0.022	0.026	0.016	0.020	0.014	0.030
Mg	0.816	0.840	0.725	0.769	0.729	0.712	1.037	1.046	1.102	0.993	1.210	0.997
Ca	0.743	0.710	0.826	0.769	0.846	0.934	0.058	0.065	0.146	0.260	0.065	0.041
Na	0.024	0.048	0.026	0.028	0.034	0.027	0.001	0.004	0.004	0.002	0.003	0.001
K	n.d.	n.d.	n.d.	n.d.	n.d.	n.d.	n.d.	n.d.	b.d.l.	b.d.l.	n.d.	n.d.
Total	4.000	4.000	4.000	4.000	4.000	4.000	4.000	4.000	4.000	4.000	4.000	4.000
Analyst	3	3	3	3	3	3	3	3	2	2	3	3

b.d.l., below detection limit; n.d., not determined. Analysts: 1, W. G. Ernst; 2, R. Berry; 3, B. Schmidt.

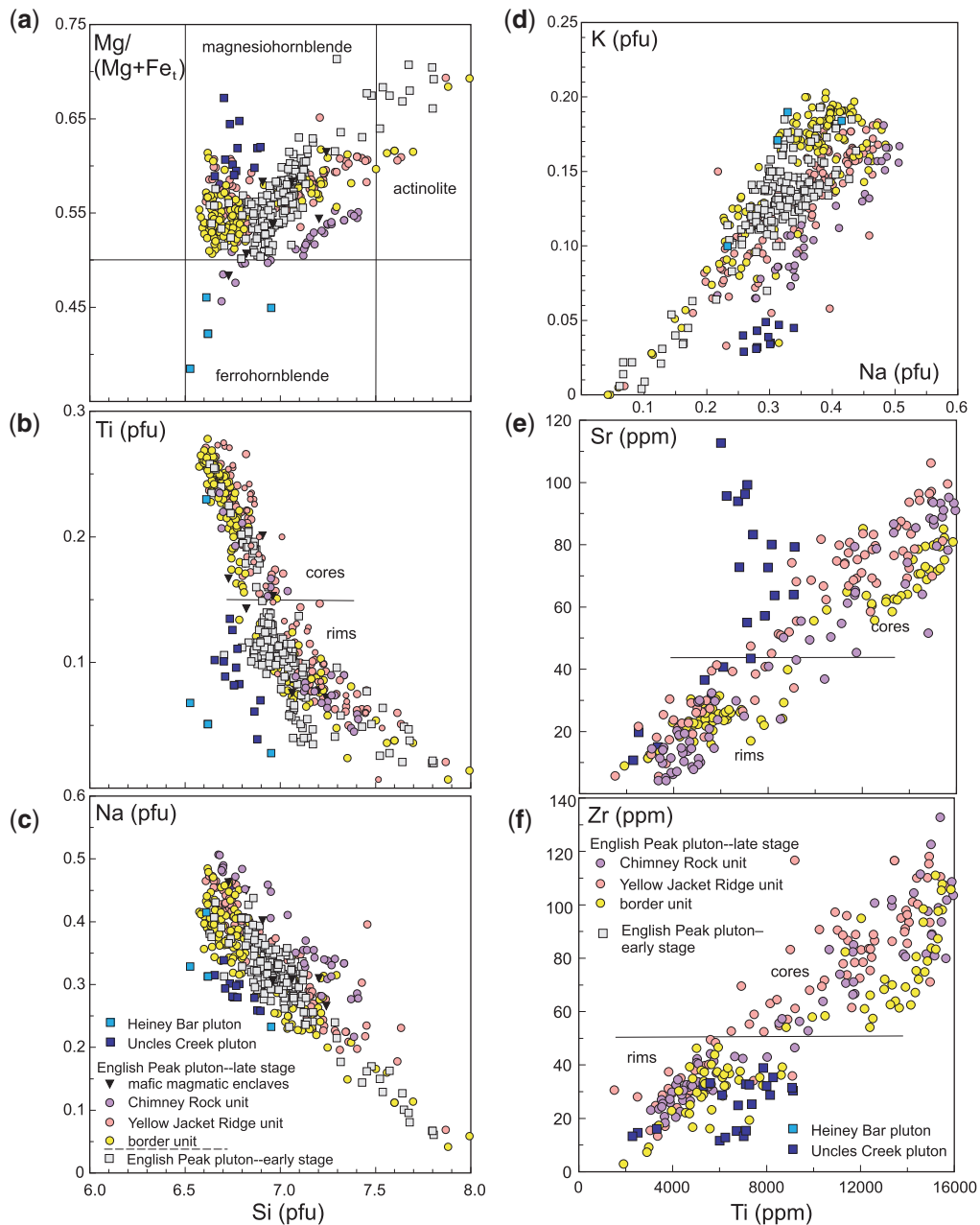


Fig. 7. Compositional variations of magnesianhornblende and actinolite. (a) $Mg/(Mg+Fe_t)$ vs Si; (b) Ti vs Si; (c) Na vs Si; (d) K vs Na; (e) Sr vs Ti; (f) Zr vs Ti. pfu, cations per formula unit.

these two plutons have REE patterns with shallow negative slopes, but sample EP-289 (69.4% SiO_2) has a steeper slope in the light REE (LREE) and the lowest middle REE (MREE) abundances (Fig. 11a). The REE abundances in the early stage of the English Peak pluton plot over a narrow range compared with the scattered major and trace element abundances in these rocks, and they fail to display regular variation with SiO_2 content (not shown). Europium anomalies are absent in all samples from the precursor satellite plutons and the early stage of the English Peak pluton (Fig. 11a).

The REE patterns of late-stage samples are similar to those from the early stage. However, within the late-

stage units, MREE and heavy REE (HREE) abundances decrease from border to Chimney Rock units, which results in a change from linear to spoon-shaped REE patterns (Fig. 11b). Weak, negative Eu anomalies are evident in the REE patterns of all but one sample; sample RBEP-021 from the border unit is distinct in having the lowest REE abundances and a positive Eu anomaly, which indicates that the sample contains cumulate plagioclase.

Most dikes and magmatic enclaves have SiO_2 contents varying from ~52.5 to 62 wt % and a broad range of $Mg/(Mg+Fe_t)$ from 0.48 to 0.68 (Fig. 9a). Major and trace element abundances vary widely among these samples, with only an indistinct correlation with SiO_2

Table 3. Representative calcic amphibole analyses.

Sample:	Uncles Creek pluton		Heiney Bar pluton		English Peak pluton, early stage							
	EP-145	EP-145	RBEP-050	RBEP-050	EP39	EP39	EP39	EP39	FPE1188	FPE1188	RBEP-010	RBEP-010
Spot:	4-3	5-1	hbl-95	hbl-r96	1-1	1-2	1-3	1-4	2-3	2-4	16	23
Location:	rim	rim	core	rim	core	mantle	mantle	rim	core	rim	core	actinolite
<i>Oxide and halogen contents (wt %)</i>												
SiO ₂	47.24	46.23	42.20	45.73	46.38	46.37	46.58	45.65	45.84	45.61	46.39	54.39
TiO ₂	0.35	0.92	0.58	0.25	1.11	1.10	0.88	0.87	1.61	0.95	1.12	0.19
Al ₂ O ₃	10.00	11.40	10.53	7.71	7.43	7.64	7.12	7.45	7.66	7.84	7.93	1.64
MnO	0.29	0.29	0.86	0.93	0.57	0.52	0.57	0.52	0.44	0.45	0.38	0.41
FeO	14.44	12.35	21.87	20.51	17.67	17.86	17.82	18.00	17.91	18.78	16.97	12.65
MgO	13.16	14.21	7.67	9.39	11.70	11.60	11.65	11.02	11.49	11.00	11.14	15.95
CaO	11.49	10.62	11.81	11.90	10.88	10.97	10.81	11.26	10.86	11.32	11.79	12.46
Na ₂ O	0.92	1.21	1.10	0.79	1.20	1.21	1.08	1.04	1.31	1.04	1.14	0.22
K ₂ O	0.16	0.25	0.97	0.52	0.77	0.76	0.67	0.76	0.75	0.78	0.77	0.03
F	0.00	0.08	n.d.	n.d.	0.05	0.02	0.14	0.10	0.19	0.19	n.d.	n.d.
Cl	0.00	0.01	n.d.	n.d.	0.10	0.08	0.08	0.08	0.05	0.04	n.d.	n.d.
Sum	98.06	97.53	97.60	97.74	97.85	98.13	97.36	96.74	98.02	97.92	97.65	97.95
<i>Cations per 23 oxygens</i>												
Si	6.880	6.704	6.528	6.953	6.939	6.921	6.995	6.930	6.854	6.859	6.935	7.806
Ti	0.039	0.101	0.068	0.028	0.124	0.124	0.099	0.100	0.181	0.108	0.126	0.020
Al	1.717	1.948	1.920	1.381	1.311	1.344	1.259	1.333	1.349	1.389	1.398	0.277
Mn	0.036	0.036	0.113	0.120	0.072	0.065	0.073	0.066	0.056	0.057	0.048	0.050
Fe	1.758	1.498	2.829	2.607	2.210	2.230	2.238	2.285	2.239	2.362	2.122	1.518
Mg	2.857	3.072	1.769	2.129	2.610	2.581	2.607	2.495	2.561	2.465	2.483	3.413
Ca	1.793	1.651	1.957	1.938	1.743	1.754	1.739	1.832	1.739	1.824	1.889	1.916
Na	0.259	0.339	0.329	0.233	0.347	0.349	0.315	0.307	0.379	0.304	0.330	0.061
K	0.029	0.045	0.190	0.100	0.146	0.144	0.128	0.147	0.142	0.150	0.147	0.006
F	0.000	0.040	n.d.	n.d.	0.026	0.011	0.067	0.049	0.090	0.090	n.d.	n.d.
Cl	0.000	0.000	n.d.	n.d.	0.026	0.021	0.020	0.021	0.010	0.010	n.d.	n.d.
Sum	15.370	15.430	15.700	15.490	15.554	15.545	15.541	15.565	15.600	15.620	15.480	15.070
English Peak pluton, late stage												
Sample:	Border unit					Yellow Jacket Ridge unit				Chimney Rock unit		
	EP-121	EP-121	EP-216	EP-216	EP-176B	EP-176B	358M	RBEP-024	RBEP-024			
Spot:	6-3	6-4	1-1	2-5	4-2	4-4	227	10-2	10-4			
Location:	core	rim	core	rim	core	rim	actinolite	core	rim			
<i>Oxide and halogen contents (wt %)</i>												
SiO ₂	45.51	47.52	44.73	48.67	45.27	49.10	54.50	44.86	47.24			
TiO ₂	1.86	0.76	2.50	0.68	2.08	0.65	0.19	1.70	0.68			
Al ₂ O ₃	8.27	6.95	9.25	5.83	8.90	5.89	1.26	8.36	5.99			
MnO	0.40	0.38	0.18	0.50	0.34	0.41	0.48	0.77	0.77			
FeO	16.78	16.89	14.41	16.91	15.76	16.09	12.72	19.23	18.52			
MgO	11.65	12.20	12.86	12.35	11.72	12.74	16.13	9.80	10.90			
CaO	11.31	11.76	11.16	11.53	11.48	11.76	11.59	11.05	11.22			
Na ₂ O	1.34	0.87	1.69	0.96	1.50	0.86	0.25	1.61	1.14			
K ₂ O	0.87	0.64	0.89	0.51	0.83	0.51	0.03	0.82	0.56			
F	0.11	0.14	0.17	0.03	0.17	0.09	n.d.	0.11	0.32			
Cl	0.07	0.03	0.04	0.03	0.05	0.03	n.d.	0.04	0.02			
Sum	98.14	98.08	97.83	98.01	98.06	98.09	97.16	98.31	97.23			
<i>Cations per 23 oxygens</i>												
Si	6.780	7.043	6.620	7.206	6.719	7.225	7.869	6.765	7.126			
Ti	0.209	0.085	0.278	0.076	0.233	0.072	0.021	0.193	0.077			
Al	1.452	1.214	1.613	1.017	1.557	1.022	0.215	1.485	1.064			
Mn	0.050	0.047	0.022	0.063	0.043	0.051	0.059	0.098	0.099			
Fe	2.090	2.093	1.784	2.094	1.957	1.980	1.535	2.425	2.336			
Mg	2.587	2.695	2.836	2.726	2.593	2.794	3.473	2.203	2.450			
Ca	1.805	1.867	1.770	1.830	1.826	1.853	1.793	1.785	1.813			
Na	0.388	0.250	0.485	0.276	0.432	0.244	0.069	0.472	0.334			
K	0.166	0.120	0.168	0.096	0.157	0.095	0.006	0.157	0.107			
F	0.050	0.070	0.080	0.010	0.080	0.040	n.d.	0.050	0.150			
Cl	0.020	0.010	0.010	0.010	0.010	0.010	n.d.	0.010	0.010			
Sum	15.600	15.490	15.670	15.410	15.610	15.390	15.040	15.650	15.570			

(Figs 9 and 10). The Cr contents of the most MgO-rich dikes and enclaves reach ~700 ppm, much higher than for any mafic sample from the rest of the EPC. Chromium is correlated with MgO (Fig. 10g), but not with CaO or FeO (not shown). Inasmuch as olivine and chromite are absent in these rocks, we conclude that the high Cr contents reflect original melt compositions and not accumulation of augite. This conclusion is supported by the fact that the Cr content of the late-stage augite is typically less than or equal to the Cr content in

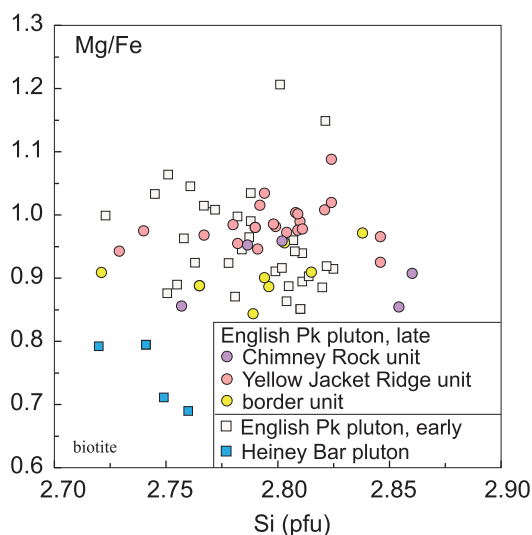


Fig. 8. Mg/Fe vs Si of biotite. pfu, cations per formula unit.

Table 4. Average biotite compositions

Unit:	Heiney Bar pluton		English Peak pluton,			English Peak pluton, late stage units					
			early stage			Border	Yellow Jacket Ridge			Chimney Rk	
Sample:	RBEP-005	RBEP-010	RBEP-011	RBEP-013	687M	RBEP-021	358M	684M	906M	RBEP-023	RBEP-022
<i>Oxides (wt %)</i>											
SiO ₂	35.13	35.96	36.18	35.66	35.95	36.25	36.40	36.36	35.88	35.56	35.91
TiO ₂	2.07	4.03	4.20	3.66	3.98	3.87	3.59	3.90	3.75	3.24	3.79
Al ₂ O ₃	15.70	14.45	13.97	13.94	13.47	14.77	14.46	13.40	13.48	14.74	13.85
Cr ₂ O ₃	0.00	0.02	0.04	0.02	0.02	0.04	0.04	0.05	0.03	0.02	0.02
FeO	22.66	20.00	20.01	20.08	20.71	19.97	19.65	20.26	19.49	20.07	20.99
MnO	0.62	0.25	0.26	0.22	0.24	0.26	0.26	0.30	0.25	0.24	0.35
MgO	9.49	10.66	11.28	11.52	10.41	10.17	10.91	10.78	11.04	11.04	10.68
CaO	0.11	0.09	0.07	0.03	0.07	0.04	0.11	0.26	0.05	0.04	0.00
Na ₂ O	0.05	0.06	0.10	0.07	0.10	0.09	0.11	0.11	0.11	0.09	0.09
K ₂ O	9.42	9.80	9.43	9.68	9.61	9.80	9.53	9.45	9.20	9.73	9.76
Total	95.25	95.26	95.54	94.85	94.54	95.20	95.06	94.86	93.29	94.77	95.45
<i>Cations per 22 oxygens</i>											
Si	5.484	5.542	5.552	5.528	5.607	5.580	5.599	5.633	5.627	5.515	5.558
Al ^{iv}	2.516	2.458	2.448	2.471	2.393	2.420	2.401	2.367	2.373	2.485	2.442
Al ^{vi}	0.374	0.167	0.079	0.077	0.085	0.261	0.222	0.081	0.119	0.210	0.087
Ti	0.243	0.467	0.485	0.427	0.466	0.448	0.415	0.454	0.443	0.378	0.442
Cr	0.000	0.002	0.003	0.001	0.001	0.003	0.003	0.004	0.002	0.002	0.002
Fe ²⁺	2.958	2.579	2.568	2.604	2.702	2.573	2.528	2.626	2.557	2.604	2.718
Mn	0.082	0.033	0.034	0.028	0.031	0.030	0.034	0.040	0.033	0.032	0.047
Mg	2.207	2.452	2.580	2.661	2.420	2.335	2.501	2.489	2.582	2.551	2.463
Ca	0.018	0.006	0.011	0.002	0.011	0.005	0.019	0.044	0.009	0.005	0.000
Ba	0.000	0.000	0.000	0.000	0.000	0.000	0.000	0.000	0.000	0.000	0.000
Na	0.015	0.019	0.029	0.022	0.030	0.028	0.033	0.032	0.034	0.028	0.027
K	1.877	1.927	1.847	1.916	1.912	1.925	1.870	1.869	1.842	1.926	1.928
Total	15.773	15.651	15.636	15.739	15.658	15.606	15.624	15.638	15.620	15.736	15.712

the mafic dikes (Fig. 10g). The REE patterns of the mafic dikes and enclaves are essentially identical to those of rocks from the early stage of the English Peak pluton (Fig. 11). Compared with the two satellite bodies, the dikes and enclaves are enriched in LREE.

Isotopic compositions

Strontium and oxygen isotope data and analytical methods were reported by Schmidt (1994). Initial ⁸⁷Sr/⁸⁶Sr ratios in nine EPC bulk-rock samples vary over a narrow range from 0.70381 to 0.70453 (Fig. 12; Table 6). The lowest values (<0.704) are from the Uncles Creek and Heiney Bar satellite plutons. Oxygen isotope ratios range from 7.7 to 10.4‰ (V-SMOW), with the lowest values from the sample of the Uncles Creek body (Fig. 12). The δ¹⁸O values are broadly correlated with bulk-rock SiO₂ contents. Three metasedimentary host-rock samples of the Eastern Hayfork terrane have ⁸⁷Sr/⁸⁶Sr (calculated at 156 Ma) bulk values ranging from 0.70781 to 0.70915 and δ¹⁸O of 13.4–13.9‰ (Table 6).

DISCUSSION

Conditions of crystallization

A pseudosection was computed for granodiorite sample EP-216 (Table 5) from the Yellow Jacket Ridge unit of the late stage of the English Peak pluton using Theriak/Domino (de Capitani & Petrakakis, 2010) and the dataset of Holland & Powell (1998). Stability

fields computed for the P - T region 100–800 MPa and 650–850°C are plotted in Fig. 13. In addition, the broad range of clin amphibole compositions analyzed in this study permits calculation of P - T values of crystallization using three approaches. The first involved the semi-quantitative thermobarometric technique of Ernst & Liu (1998), which employs experiment-based TiO_2 and Al_2O_3 isopleths of synthetic clin amphiboles crystallized from East Pacific Rise basalt. The Ernst & Liu (1998) method generally results in P estimates of 200 MPa or lower, and T values from 610 to 675°C, although hornblende from the Heiney Bar pluton and a sample from the early stage of the English Peak pluton

yield P estimates of 550 MPa and 400 MPa, respectively. With one exception, all late-stage samples gave T of 580–765°C. In summary, this method yields P estimates lower than the 200–300 MPa pressure range determined from contact metamorphic assemblages (Hacker *et al.*, 1992; Ernst, 1999). Amphiboles classified as actinolite yielded T estimates of 430–580°C.

The second approach employed the method of Anderson & Smith (1995), which uses the clin amphibole–plagioclase exchange reactions of Holland & Blundy (1994). This approach yields P - T estimates of 360 MPa and 760°C for the Heiney Bar pluton. However, P - T estimates for early stage samples of the English

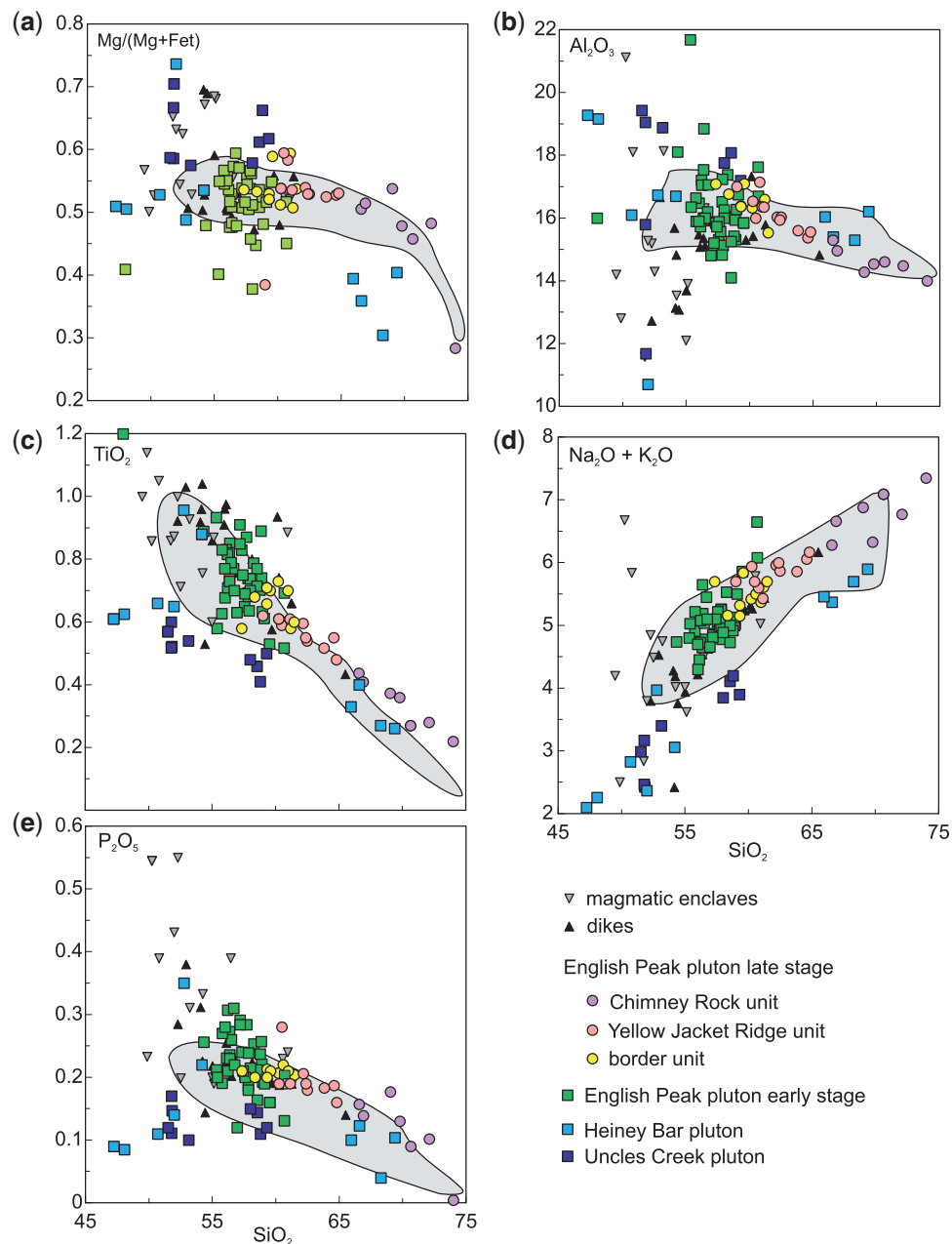


Fig. 9. Major element bulk-rock compositions. Oxides as wt %. Shaded areas represent the compositional range of the upper zone of the Wooley Creek batholith.

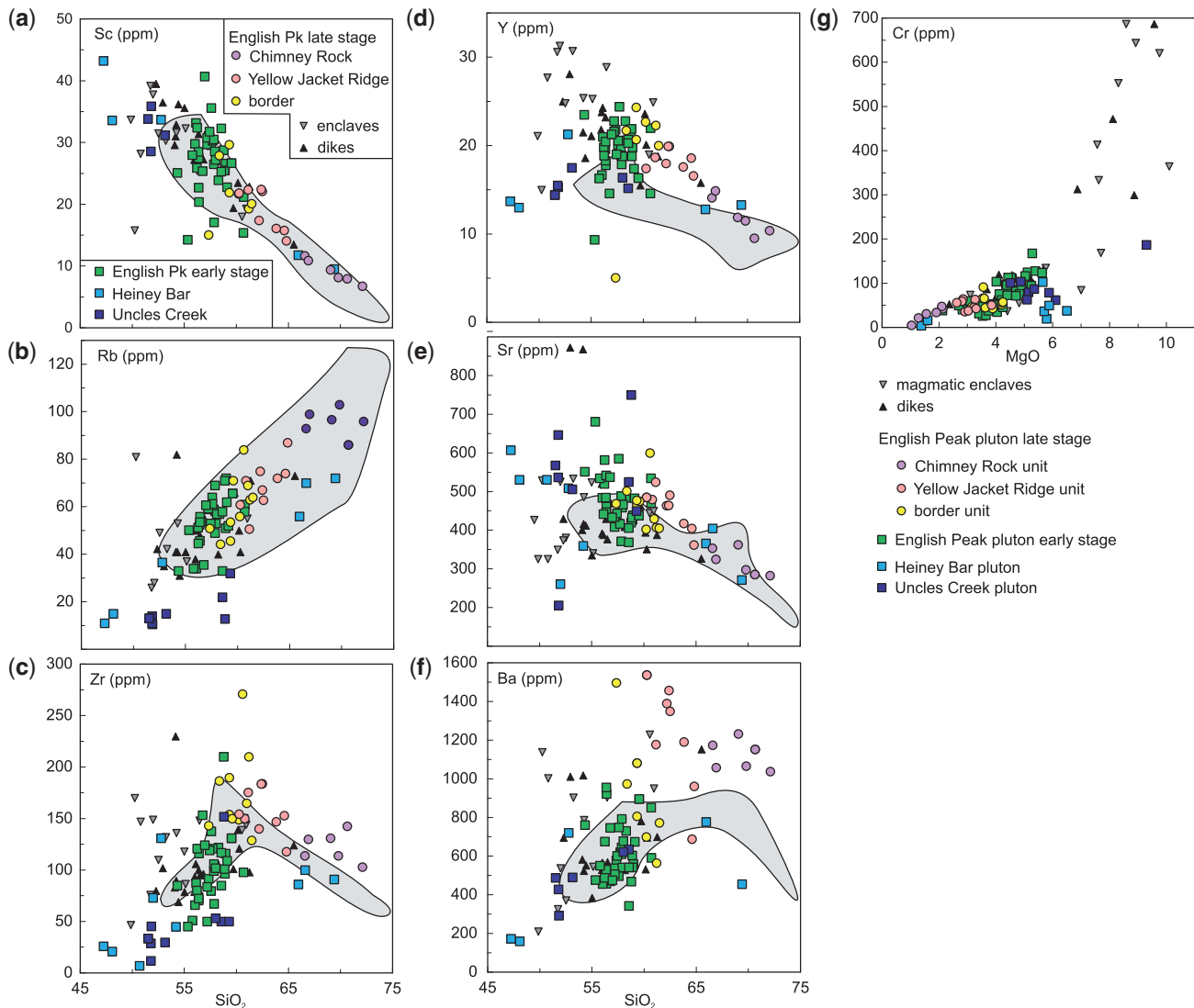


Fig. 10. (a–f) Trace element bulk-rock compositions vs SiO_2 in wt %. (g) Cr vs MgO in wt %. Gray-shaded areas are the compositional fields of the upper zone of the Wooley Creek batholith.

Peak pluton scatter widely, and some are below the computed H_2O -saturated solidus (Fig. 13; Supplementary Data Table 2). Although computed values for late-stage samples of the English Peak pluton yield P – T estimates above the solidus, pressures are generally lower than those estimated from contact metamorphic assemblages. These low P estimates are, at least in part, thought to result from difficulty in determining which compositional zones in hornblende and plagioclase pairs (if any) represent equilibrium assemblages. Amphiboles classified as actinolite yielded T estimates of 494–630°C.

The third approach determined pressure using the Al-in-hornblende calibration of Schmidt (1992) and temperature using the P -independent algorithm of Putirka (2016). This approach yielded P estimates for the Uncles Creek and Heiney Bar plutons of 590 and 510 MPa, and T estimates of 801 and 756°C, respectively (Fig. 13; Supplementary Data Table 2). These P – T ranges are

plotted in Fig. 13 for comparison purposes only, inasmuch as the pseudosection was computed for a more felsic composition. If the P estimates are correct, the fact that they are higher than the 200–300 MPa emplacement pressure (see above) suggests that hornblende crystals in these satellite plutons crystallized in deeper magma chambers. In contrast, hornblende from the early stage of the English Peak pluton gives P in the range of 270–390 MPa, at the high end of the range of contact metamorphic conditions, and T from 733 to 790°C. We found no core-to-rim variations in P – T estimates among the early stage hornblendes (Fig. 13; Supplementary Data Table 2), consistent with hornblende occurring as a low- T peritectic phase in early stage magmas. Hornblende from the late-stage units of the English Peak pluton yields distinct P – T estimates, reflecting the color of the crystals. Olive-brown cores yield P – T estimates of *c.* 450 MPa and *c.* 813°C for the border unit, *c.* 410 MPa and *c.* 812°C for the Yellow Jacket Ridge unit, and *c.* 315 MPa and *c.*

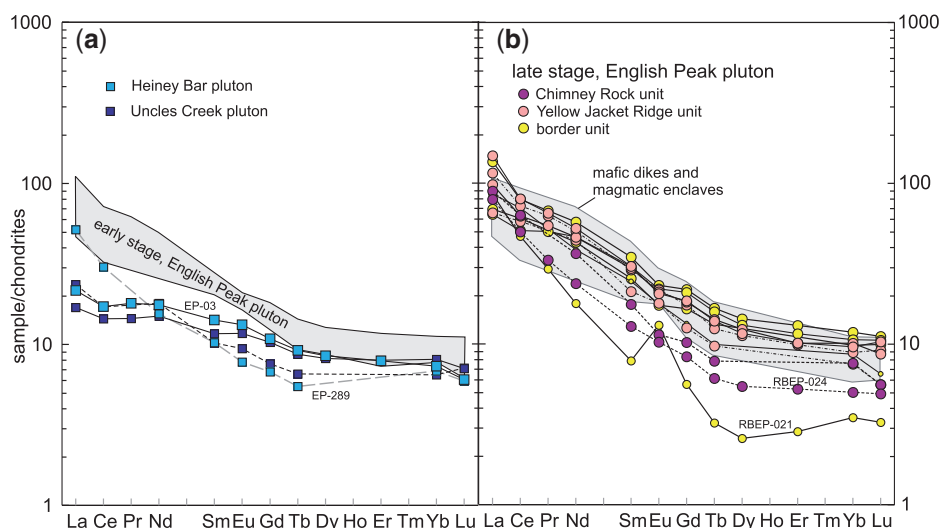


Fig. 11. Rare earth element patterns for EPC bulk-rocks normalized to chondrite (Boynton, 1984). (a) Heiney Bar and Uncles Creek plutons compared with the early stage English Peak pluton. (b) Late-stage English Peak pluton compared with the field of mafic dykes and magmatic enclaves.

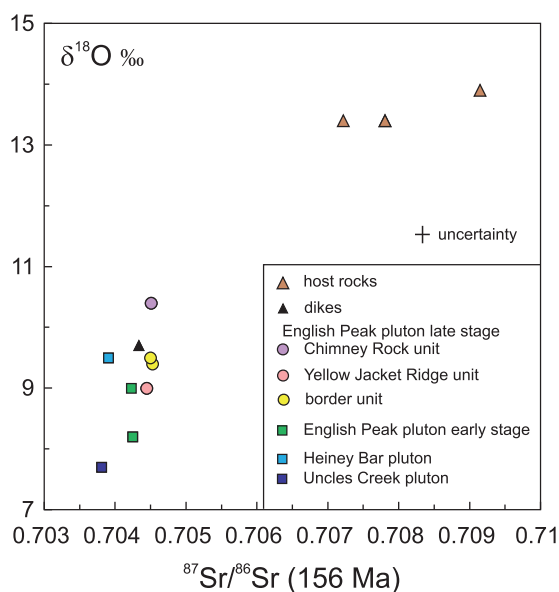


Fig. 12. Variation of $^{87}\text{Sr}/^{86}\text{Sr}$ at 156 Ma vs $\delta^{18}\text{O}$. All data are bulk-rock compositions.

775°C for the Chimney Rock unit (Supplementary Data Table 2). Green rim compositions give *c.* 280 MPa and *c.* 740°C (border unit), *c.* 220 MPa and *c.* 728°C (Yellow Jacket Ridge unit), and *c.* 150 MPa and *c.* 703°C (Chimney Rock unit). Comparison with the computed phase stability fields (Fig. 13) indicates that the hornblende cores represent *P*–*T* conditions in the field of biotite stability, whereas the lower *T* rims grew in equilibrium with biotite + quartz. Amphiboles classified as actinolite yielded *T* estimates of ~635–684°C. These latter estimates are consistent with subsolidus replacement of magmatic hornblende, both olive–brown cores and medium green rims, by actinolite.

Uncles Creek pluton

The textures of these samples, containing euhedral prisms of hornblende and interstitial plagioclase, indicate crystallization from an H_2O -rich magma at moderate to high *P* (e.g. Egger, 1972; Allen & Boettcher, 1978, 1983; Naney, 1983)—conditions that would suppress plagioclase stability. Such growth would explain the unusually high Sr contents in Uncles Creek hornblende (Fig. 7) because Sr would not be sequestered in plagioclase at the hornblende liquidus. The *P* estimate of *c.* 590 MPa fits this explanation, and indicates that crystallization of Uncles Creek magmas began at depths well below the final level of emplacement.

Early stage, English Peak pluton

In contrast to the satellite bodies, *P* estimates from hornblende in early stage English Peak samples overlap with pressures of emplacement based on contact metamorphic conditions (200–300 MPa). This overlap is broadly consistent with amphibole crystallization after emplacement, as indicated by hornblende textures, which are characteristic of near-solidus peritectic reaction from augite and opx.

Late stage, English Peak pluton

The conditions of crystallization for olive–brown hornblende cores from the border and Yellow Jacket Ridge units of the late stage of the English Peak pluton (*c.* 420 MPa, 810°C) indicate a somewhat lower temperature than suggested by comparison with the computed pseudosection, in which the hornblende stability field extends to higher *T* (Fig. 13). In contrast, the conditions of crystallization of green hornblende rims are consistent with the pseudosection and textural data, both of which indicate that hornblende rims show coherent contacts with biotite, plagioclase, and quartz (Fig. 5c

Table 5. Representative bulk-rock analyses

Sample:	Uncles Creek pluton				Heiney Bar pluton			
	177M	180M	EP-141	EP-145	EP-003	EP-6	66M	67M
<i>Major oxides (wt %)</i>								
SiO ₂	53.15	58.80	58.54	51.51	47.25	65.95	54.20	52.00
TiO ₂	0.54	0.41	0.46	0.57	0.61	0.33	0.88	0.65
Al ₂ O ₃	18.88	16.70	18.08	19.43	19.28	16.04	16.70	10.70
Fe ₂ O ₃	7.54	6.15	6.13	8.17	11.21	4.86	9.80	10.00
MnO	0.15	0.12	0.13	0.15	0.16	0.12	0.20	0.18
MgO	5.15	6.10	4.88	5.87	5.88	1.60	5.70	14.10
CaO	8.93	7.15	7.48	9.9	12.65	4.64	9.10	9.60
Na ₂ O	2.70	3.00	3.10	2.26	1.4	3.12	1.75	1.35
K ₂ O	0.70	1.20	1.01	0.73	0.7	2.34	1.31	1.02
P ₂ O ₅	0.10	0.11	0.14	0.12	0.09	0.10	0.22	0.14
LOI	2.17	1.63	n.d.	2.41	1.5	0.92	n.d.	n.d.
Total	100.02	99.85	99.96	101.12	100.73	100.01	99.93	99.91
<i>Trace elements (ppm)</i>								
Sc	31.2	n.d.	25.1	33.9	43.2	11.8	n.d.	n.d.
V	207	n.d.	165	237	382	91	n.d.	n.d.
Cr	80	62	104	79	50	17	37	981
Ni	45	32	54	63	b.d.l.	15	20	219
Cu	58	51	50	b.d.l.	159	5	60	80
Zn	78	60	68	83	75	70	98	81
Ga	n.d.	n.d.	n.d.	15.2	14.0	n.d.	n.d.	n.d.
Rb	15	13	22	13.1	11.1	56	n.d.	n.d.
Sr	506	750	526	568.0	607.2	366	360	261
Y	17.5	n.d.	15.2	14.4	13.7	12.8	n.d.	n.d.
Zr	30	152	50	33.6	26.0	86	45	73
Nb	12	n.d.	5	1.7	2.2	8	n.d.	n.d.
Ba	491	n.d.	636	488.0	173.4	777	n.d.	n.d.
La	n.d.	n.d.	7.30	5.24	6.69	n.d.	n.d.	n.d.
Ce	n.d.	n.d.	13.80	11.65	13.84	n.d.	n.d.	n.d.
Pr	n.d.	n.d.	n.d.	1.77	2.20	n.d.	n.d.	n.d.
Nd	n.d.	n.d.	10.80	9.00	10.57	n.d.	n.d.	n.d.
Sm	n.d.	n.d.	1.99	2.27	2.76	n.d.	n.d.	n.d.
Eu	n.d.	n.d.	0.69	0.86	0.97	n.d.	n.d.	n.d.
Gd	n.d.	n.d.	n.d.	2.66	2.81	n.d.	n.d.	n.d.
Tb	n.d.	n.d.	0.31	0.41	0.43	n.d.	n.d.	n.d.
Dy	n.d.	n.d.	n.d.	2.63	2.73	n.d.	n.d.	n.d.
Er	n.d.	n.d.	n.d.	1.67	1.66	n.d.	n.d.	n.d.
Yb	n.d.	n.d.	1.35	1.69	1.53	n.d.	n.d.	n.d.
Lu	n.d.	n.d.	0.23	0.23	0.19	n.d.	n.d.	n.d.
Hf	n.d.	n.d.	n.d.	1.04	0.99	n.d.	n.d.	n.d.
Ta	n.d.	n.d.	n.d.	0.09	1.71	n.d.	n.d.	n.d.
Th	n.d.	n.d.	n.d.	0.72	1.17	n.d.	n.d.	n.d.
U	n.d.	n.d.	n.d.	0.29	0.37	n.d.	n.d.	n.d.
Data source	1	1	2	3	3	2	1	1

(continued)

and d). The P estimates determined on the basis of hornblende rim compositions, $c.$ 250 MPa, overlap with those of the early stage and are essentially identical to P estimates of emplacement based on contact metamorphic assemblages. Although the pressure difference suggested by distinct core and rim compositions could be the result of crystal chemical effects or a lack of an appropriate equilibrium assemblage (e.g. Anderson & Smith, 1995), the sharp core-to-rim transition and the fact that the core hornblende is embayed by rim hornblende (Fig. 5d) strongly suggest a change in conditions of crystallization. We suggest that the simplest interpretation is that hornblende cores crystallized in a magma reservoir a few kilometers ($c.$ 5 km) below the level of emplacement. Rise of the magmas to the final emplacement level was accompanied by partial resorption,

which formed embayments in the core hornblende. Final solidification of the magmas resulted in hornblende rim formation at T a few tens of degrees above the H₂O-saturated solidus.

Zircon saturation temperatures (Boehnke *et al.*, 2013) were computed for all analyzed samples of the EPC. All early stage samples yield $T < 665^{\circ}\text{C}$, which probably results from a combination of very low- T zircon saturation and the cumulate compositions of these rocks (see below). The maximum zircon saturation T for late-stage samples is 717°C and most samples have saturation temperatures $< 700^{\circ}\text{C}$.

Relationships among magmatic units

Samples from all three EPC plutons with < 60 wt % SiO₂ display significant compositional scatter (Fig. 9). This

Table 5. Continued

Sample:	English Peak pluton, early stage						
	EP-039	FPE-588	FPE-688	FPE-1188	RBEP-010	RBEP-011	RBEP-013
<i>Major oxides (wt %)</i>							
SiO ₂	56.38	56.97	59.53	56.76	57.42	57.6	56.23
TiO ₂	0.73	0.63	0.53	0.7	0.75	0.69	0.71
Al ₂ O ₃	17.54	14.81	15.85	17.06	15.73	15.89	17.05
Fe ₂ O ₃	7.72	8.37	6.41	8.06	8.16	7.8	7.84
MnO	0.13	0.14	0.11	0.13	0.14	0.13	0.13
MgO	3.65	5.63	3.93	3.74	4.4	4.71	4.25
CaO	6.53	7.91	6.24	7.08	7.13	6.66	7.26
Na ₂ O	3.27	2.62	3.12	3.46	2.92	2.92	3.21
K ₂ O	2.38	2.04	2.74	1.64	2.18	2.3	1.87
P ₂ O ₅	0.23	0.12	0.16	0.22	0.21	0.2	0.21
LOI	1.27	0.39	0.92	0.84	0.65	1.77	0.59
Total	99.84	99.63	99.54	99.68	99.03	98.89	98.76
<i>Trace elements (ppm)</i>							
Sc	22.7	40.7	26.7	25.4	31.8	35.6	32.4
V	179	207	163	194	215	196	197
Cr	28	124	51	38	73	72	46
Ni	7	23	24	9	10	18	12
Cu	81	106	128	b.d.l.	17	b.d.l.	25
Zn	85	83	70	88	85	77	82
Ga	17.7	14.9	15.9	17.1	15.8	15.9	16.3
Rb	53.6	60.7	65.7	35.6	53.0	61.3	44.7
Sr	542.1	433.8	437.9	537.8	443.7	585.4	581.9
Y	20.5	21.3	16.4	14.6	19.0	20.6	18.9
Zr	72.3	124.3	131.1	153.4	119.3	137.7	120.9
Nb	6.7	5.5	5.9	5.9	7.2	5.8	5.3
Ba	956.8	476.1	896.5	747.0	602.4	749.9	676.1
La	34.30	19.21	22.72	29.24	17.59	22.78	21.49
Ce	58.14	33.73	41.49	46.02	34.08	38.14	36.03
Pr	7.56	4.79	5.38	5.68	4.66	5.61	5.08
Nd	29.43	21.10	21.32	21.81	20.45	24.61	22.96
Sm	5.40	4.80	4.39	3.97	4.74	5.41	4.91
Eu	1.55	1.22	1.25	1.38	1.29	1.44	1.43
Gd	4.67	4.65	3.69	3.23	4.25	4.66	4.50
Tb	0.60	0.68	0.51	0.45	0.60	0.67	0.61
Dy	3.72	4.10	3.44	2.80	3.61	3.87	3.64
Er	2.31	2.43	1.81	1.54	2.16	2.25	2.21
Yb	2.35	2.30	1.87	1.63	2.08	2.07	2.05
Lu	0.35	0.35	0.23	0.27	0.29	0.30	0.31
Hf	2.36	3.61	3.50	4.05	3.23	3.82	3.26
Ta	0.45	0.40	0.46	0.46	0.49	0.43	0.36
Th	7.46	7.57	6.41	5.44	5.24	7.00	6.27
U	0.90	1.45	1.02	1.11	1.51	1.19	1.34
Data source	3	4	4	4	4	4	4

(continued)

scatter may be explained in part as the result of variable accumulation of pyroxenes, plagioclase, and perhaps amphibole. It could also be explained as the result of episodic emplacement of diverse mafic to intermediate magmas. The potential for emplacement of diverse magmas is exemplified by comparison of the Uncles Creek pluton, typified by its prominent euhedral hornblende, distinctly higher Mg/(Mg + Fe_t), and lower total alkalis, TiO₂, Rb, Zr, and Y, with the younger English Peak pluton (Figs 9 and 10). Early hornblende stability in the Uncles Creek body indicates crystallization from an H₂O-rich magma. In contrast, in the Heiney Bar pluton and particularly in the early stage of the English Peak pluton, pyroxenes are the high-*T* ferromagnesian minerals. Moreover, some samples of the early stage of the English Peak pluton lack magmatic hornblende. These features indicate that Heiney Bar and early stage

English Peak plutons were constructed from multiple magma batches that contained variable H₂O contents, and that nearly all early stage English Peak magmas had lower H₂O contents than the Uncles Creek magmas.

Some of the compositional scatter among samples from the early stage of the English Peak pluton, particularly in terms of Mg/(Mg + Fe_t) and Al₂O₃, probably reflects accumulation of pyroxenes and plagioclase. Pyroxenes in early stage rocks have Mg/(Mg + Fe_t) of 0.67–0.76 (augite) and 0.54–0.60 (opx). The augite/bulk-rock Fe–Mg *K_D* values calculated for early stage samples lie in the range 0.46–0.71, too high for augite to be in equilibrium with a melt of the same composition as the bulk-rock (e.g. Putirka, 2008). This discrepancy is readily explained if the bulk-rock compositions reflect pyroxene accumulation. Therefore, early stage samples

Table 5. Continued

Sample:	English Peak pluton, late stage							
	Border unit							
	EP-121	EP-126	EP-209A	EP-267	RBEP-021	31M	33M	34M
<i>Major oxides (wt %)</i>								
SiO ₂	59.32	58.36	61.20	61.47	57.35	59.60	61.00	58.80
TiO ₂	0.71	0.68	0.58	0.60	0.58	0.70	0.70	0.80
Al ₂ O ₃	16.37	16.77	16.60	15.54	17.09	17.10	16.36	16.30
Fe ₂ O ₃	6.61	6.66	6.07	6.07	6.66	5.80	5.76	6.86
MnO	0.1	0.11	0.11	0.11	0.14	0.11	0.10	0.12
MgO	3.63	3.84	3.16	3.56	3.89	4.20	4.25	4.85
CaO	6.52	6.95	6.06	6.09	6.95	6.30	6.20	6.96
Na ₂ O	3.07	3.18	3.48	3.08	3.3	3.30	2.95	2.92
K ₂ O	2.08	1.98	2.13	2.62	2.4	2.54	2.42	2.02
P ₂ O ₅	0.2	0.2	0.20	0.20	0.21	0.21	0.21	0.23
LOI	0.76	0.9	n.d.	n.d.	0.66	n.d.	n.d.	n.d.
Total	98.61	98.74	99.59	99.35	98.56	99.95	100.04	99.95
<i>Trace elements (ppm)</i>								
Sc	29.7	27.9	19.3	20.1	15.1	n.d.	n.d.	n.d.
V	169	173	138	141	154	n.d.	n.d.	n.d.
Cr	45	52	47	92	43	57	58	60
Ni	16	13	8	12	16	30	32	30
Cu	34	104	27	32	126	50	65	60
Zn	71	74	63	61	77	78	78	86
Ga	16.2	16.6	n.d.	n.d.	16.3	n.d.	n.d.	n.d.
Rb	45.7	44.2	63	64	51.0	71	69	54
Sr	477.4	501.8	408	406	469.0	475	430	420
Y	24.3	21.7	22.3	20.0	5.0	n.d.	n.d.	n.d.
Zr	189.8	186.6	210	129	143.2	150	165	150
Nb	7.9	7.3	10	10	4.8	n.d.	n.d.	n.d.
Ba	1081.8	974.4	566	773	1497	n.d.	n.d.	n.d.
La	42.19	19.85	21.40	n.d.	26.55	n.d.	n.d.	n.d.
Ce	64.15	40.99	48.90	n.d.	37.86	n.d.	n.d.	n.d.
Pr	8.23	6.12	n.d.	n.d.	3.58	n.d.	n.d.	n.d.
Nd	34.38	27.84	25.80	n.d.	10.74	n.d.	n.d.	n.d.
Sm	6.77	5.92	4.98	n.d.	1.53	n.d.	n.d.	n.d.
Eu	1.70	1.62	1.28	n.d.	0.96	n.d.	n.d.	n.d.
Gd	5.65	5.43	n.d.	n.d.	1.45	n.d.	n.d.	n.d.
Tb	0.79	0.75	0.63	n.d.	0.15	n.d.	n.d.	n.d.
Dy	4.62	4.21	n.d.	n.d.	0.83	n.d.	n.d.	n.d.
Er	2.74	2.43	n.d.	n.d.	0.60	n.d.	n.d.	n.d.
Yb	2.48	2.22	2.05	n.d.	0.73	n.d.	n.d.	n.d.
Lu	0.36	0.34	0.32	n.d.	0.10	n.d.	n.d.	n.d.
Hf	4.80	4.63	n.d.	n.d.	3.46	n.d.	n.d.	n.d.
Ta	4.04	0.45	n.d.	n.d.	0.38	n.d.	n.d.	n.d.
Th	12.04	2.40	n.d.	n.d.	6.49	n.d.	n.d.	n.d.
U	1.06	1.05	n.d.	n.d.	1.51	n.d.	n.d.	n.d.
Data source	3	3	2	2	4	1	1	1

(continued)

with high Mg/(Mg + Fe_t) and low Al₂O₃ are most probably pyroxene cumulates. However, a number of early stage samples have low Mg/(Mg + Fe_t) over a wide range of SiO₂ (47–61 wt %; Fig. 9a). Accumulation of mafic silicates ± plagioclase ± Fe–Ti oxides cannot explain these compositions because the mafic silicates have high Mg/(Mg + Fe_t), and TiO₂ is not correlated with Mg/(Mg + Fe_t) (not shown). Instead, we note that the Mg/(Mg + Fe_t) values of mafic dikes in the EPC span nearly the same range as those for the early stage rocks. Therefore, although some of the variability within the early stage of the English Peak pluton is due to accumulation of pyroxene ± plagioclase, much of the

variability reflects construction of the early stage from numerous magma pulses that spanned a broad range of Mg/(Mg + Fe_t) values. Episodic construction of the early stage is consistent with the lack of discernible zonation of rock types at the map scale (Fig. 3).

A direct genetic relationship between early and late-stage magmas of the English Peak pluton is unlikely for at least two reasons. First, we have argued that the early stage represents a collection of many magma batches, characterized by a rather wide range of bulk-rock compositions. Second, the initial ⁸⁷Sr/⁸⁶Sr ratios and δ¹⁸O values of two early stage samples are slightly

Table 5. Continued

Sample:	English Peak pluton, late stage						
	Yellow Jacket Ridge unit						
	185M	EP-155	EP-176B	EP-216	EP-219	RBEP-023	24M
<i>Major oxides (wt %)</i>							
SiO ₂	60.60	62.49	60.26	62.38	64.61	61.13	60.80
TiO ₂	0.60	0.54	0.61	0.55	0.55	0.61	0.60
Al ₂ O ₃	16.55	16.03	16.54	15.94	15.38	16.35	17.15
Fe ₂ O ₃	5.70	5.12	5.62	5.33	5.05	5.54	5.45
MnO	0.10	0.09	0.09	0.09	0.10	0.09	0.10
MgO	4.20	2.91	3.31	3.03	2.85	3.23	3.85
CaO	6.33	5.51	6.01	5.33	5.20	6.12	6.20
Na ₂ O	3.05	3.18	3.08	3.16	3.33	3.22	3.10
K ₂ O	2.45	2.69	2.86	2.84	2.73	2.21	2.50
P ₂ O ₅	0.22	0.18	0.19	0.19	0.19	0.19	0.19
LOI	0.74	1.15	0.92	0.75	n.d.	1.1	n.d.
Total	99.90	99.89	99.49	98.84	99.99	98.69	100.03
<i>Trace elements (ppm)</i>							
Sc	n.d.	22.1	21.8	22.4	15.8	22.4	n.d.
V	n.d.	118	133	120	105	129	n.d.
Cr	52	36	43	38	65	46	51
Ni	14	10	16	12	14	14	30
Cu	42	b.d.l.	136	13	18	100	60
Zn	59	58	62	67	61	67	72
Ga	n.d.	15.7	15.5	15.1	n.d.	16.4	n.d.
Rb	84	62.8	60.9	67.1	74	50.6	71
Sr	600	491.1	485.7	464.6	405	525.0	480
Y	n.d.	19.9	17.4	19.9	18.6	18.7	n.d.
Zr	271	184.0	154.5	183.7	153	175.6	150
Nb	n.d.	8.4	8.3	8.1	12	8.1	n.d.
Ba	n.d.	1350	1538	1458	689	1178	n.d.
La	n.d.	45.98	24.81	30.41	n.d.	35.90	n.d.
Ce	n.d.	64.62	43.97	50.42	n.d.	58.42	n.d.
Pr	n.d.	7.97	5.97	6.64	n.d.	7.65	n.d.
Nd	n.d.	31.44	25.01	27.73	n.d.	30.17	n.d.
Sm	n.d.	5.95	5.15	5.75	n.d.	5.63	n.d.
Eu	n.d.	1.51	1.61	1.55	n.d.	1.60	n.d.
Gd	n.d.	4.82	4.49	4.72	n.d.	4.53	n.d.
Tb	n.d.	0.66	0.57	0.67	n.d.	0.59	n.d.
Dy	n.d.	3.74	3.60	3.97	n.d.	3.64	n.d.
Er	n.d.	2.13	1.95	2.12	n.d.	2.07	n.d.
Yb	n.d.	2.01	1.70	2.11	n.d.	1.85	n.d.
Lu	n.d.	0.33	0.29	0.28	n.d.	0.29	n.d.
Hf	n.d.	4.85	3.84	4.97	n.d.	4.51	n.d.
Ta	n.d.	4.84	5.77	0.68	n.d.	0.68	n.d.
Th	n.d.	15.71	5.43	10.36	n.d.	11.87	n.d.
U	n.d.	3.62	1.40	1.51	n.d.	2.04	n.d.
Data source	1	3	3	3	2	4	1

(continued)

lower than those of four late-stage samples (Fig. 12). Therefore, even if early stage magmas differentiated and coalesced to yield magmas of the late stage, such differentiation must have involved assimilation of crustal rocks, for which there is no field or petrographic evidence at the exposed level of emplacement.

Compared with the early stage, compositional variation within the late stage of the English Peak pluton is well defined, with regular variation in many elements as a function of increasing SiO₂ (Figs 9–11). This type of zonation toward more evolved interior compositions has classically been ascribed to *in situ* fractional crystallization (e.g. Bateman & Chappell, 1979). In this

scenario, decreasing Al₂O₃, Mg/(Mg + Fe_t), TiO₂, P₂O₅, Sc, Y, Zr, and MREE and HREE (Figs 9–11) would suggest fractionation of plagioclase, hornblende, apatite, zircon, and Fe–Ti oxide(s). Although *in situ* fractional crystallization accounts for much of the bulk-rock geochemical variation within late-stage samples, it fails to explain why Sr abundances in the border unit are as low as or lower than in other late stage units (Fig. 10d), or why Ba abundances in late-stage samples are so scattered (Fig. 10f). If the border, Yellow Jacket Ridge and Chimney Rock units were comagmatic, then the decrease in Al₂O₃ contents from the border unit to the Chimney Rock unit would imply fractionation of

Table 5. Continued

Sample:	English Peak pluton, late stage			
	Chimney Rock unit			
	EP-163	EP-169	EP-221	RBEP-024
<i>Major oxides (wt %)</i>				
SiO ₂	69.80	69.05	66.59	70.66
TiO ₂	0.36	0.37	0.44	0.27
Al ₂ O ₃	14.54	14.28	15.30	14.61
Fe ₂ O ₃	3.37	3.25	4.15	2.44
MnO	0.07	0.08	0.08	0.05
MgO	1.56	1.91	2.14	1.04
CaO	3.17	3.73	4.11	2.39
Na ₂ O	3.27	3.74	3.30	3.15
K ₂ O	3.06	3.14	2.98	3.94
P ₂ O ₅	0.13	0.18	0.16	0.09
LOI	0.66	0.75	n.d.	0.83
Total	99.99	100.48	99.25	98.64
<i>Trace elements (ppm)</i>				
Sc	8.2	9.4	11.7	8.0
V	54	62	76	56
Cr	31	34	42	5
Ni	7	10	12	10
Cu	12	10	11	33
Zn	37	42	46	43
Ga	n.d.	n.d.	n.d.	14.5
Rb	103	97	93	86.1
Sr	298	363	354	286.0
Y	11.5	11.9	14.1	9.5
Zr	114	131	114	142.6
Nb	3	n.d.	7	7.8
Ba	1066	1233	1174	1153
La	27.70	n.d.	n.d.	24.60
Ce	51.20	n.d.	n.d.	40.22
Pr		n.d.	n.d.	4.05
Nd	21.90	n.d.	n.d.	14.26
Sm	3.44	n.d.	n.d.	2.51
Eu	0.84	n.d.	n.d.	0.76
Gd	n.d.	n.d.	n.d.	2.16
Tb	0.37	n.d.	n.d.	0.29
Dy	n.d.	n.d.	n.d.	1.76
Er	n.d.	n.d.	n.d.	1.10
Yb	1.59	n.d.	n.d.	1.04
Lu	0.18	n.d.	n.d.	0.16
Hf	n.d.	n.d.	n.d.	3.79
Ta	n.d.	n.d.	n.d.	0.69
Th	n.d.	n.d.	n.d.	17.85
U	n.d.	n.d.	n.d.	1.99
Data source	2	2	2	4

LOI, loss on ignition; n.d., not determined; b.d.l., below detection limits. Data sources: 1, XRF, Ernst (1998); 2, inductively coupled plasma atomic emission spectrometry and instrumental neutron activation analysis for REE, Schmidt (1994); 3, Schmidt samples reanalyzed by XRF (major elements) and LA-ICP-MS (trace elements) by R. Berry; 4, XRF (major elements) and LA-ICP-MS (trace elements) by R. Berry.

plagioclase. However, plagioclase fractionation should also result in regular decrease in Sr abundances from border to Chimney Rock units, which is not the case. It is noteworthy that lower Sr abundances of border unit magmas are reflected in lower Sr contents in hornblende from the border unit, compared with other late-stage units (Fig. 7e). Thus we tentatively conclude that although minor fractional crystallization may have

occurred at the level of emplacement, such *in situ* fractionation was not responsible for inward zonation of the late-stage magmas.

The wide scatter of Ba contents in border and Yellow Jacket Ridge units is striking when compared with Ba variation in the neighboring Wooley Creek batholith (Fig. 10f). This broad range of compositions cannot be explained by accumulation of K-feldspar—an interstitial phase in all but the most evolved samples. Although accumulation, or deuteric chloritization, of biotite might explain the scatter in Ba contents, such accumulation or alteration should result in widely variable Rb concentrations, and in either case correlation of Rb and Ba would be expected; however, no such correlation exists (not shown). We therefore hypothesize that the measured variability in Ba in the border and Yellow Jacket Ridge units reflects percolation of Ba-rich melt through mushy late-stage magmas during the final stages of solidification. This idea is consistent with the interstitial to poikilitic habits of K-feldspar in these two units and with computed phase relationships (Fig. 13), which indicate that K-feldspar crystallized at or near the solidus.

Petrological development of the English Peak plutonic complex

Plutons of the EPC span Middle to Late Jurassic time, a time marked by the Siskiyou orogenic event. The new U–Pb (zircon) age data (Ernst *et al.*, in preparation) indicate that the *c.* 172 Ma Uncles Creek pluton pre-dates contractional tectonism and regional metamorphism of the Siskiyou orogeny (*c.* 170–168 Ma; Coleman *et al.*, 1988; Garlick *et al.*, 2009; Medaris *et al.*, 2009), whereas the Heiney Bar (*c.* 166 Ma) and English Peak plutons (*c.* 160–155 Ma) post-date this event. The pre-Siskiyou age of the Uncles Creek pluton makes it coeval with the Western Hayfork arc (Hacker *et al.*, 1995; Donato *et al.*, 1996), deposits of which are characterized by magmatic amphibole (Barnes & Barnes, 2013, and unpublished data). We thus infer that parental magmas to the Uncles Creek pluton were H₂O-rich arc magmas that ponded and differentiated in the pre-Siskiyou Klamath deep crustal section (Fig. 14).

The post-Siskiyou ages of both the Heiney Bar and English Peak plutons make them part of Wooley Creek suite of plutons (Barnes *et al.*, 1992; Allen & Barnes, 2006). This intrusive suite was emplaced in a retro-arc setting and is typified by higher initial ⁸⁷Sr/⁸⁶Sr and δ¹⁸O values and lower ε_{Nd} values than expected from a depleted mantle source, as noted by Barnes *et al.* (1992) and Allen & Barnes (2006). Those researchers interpreted the isotopic data to indicate that mafic magmas parental to Wooley Creek suite plutons were modified by deep crustal assimilation of—and/or mixing with—partial melts of lower crustal metasedimentary rocks (Barnes *et al.*, 1990; Allen & Barnes, 2006). The ranges

Table 6. Sr and oxygen isotope compositions

Sample	Rock type	SiO ₂ (wt %)	Rb (ppm)	Sr (ppm)	⁸⁷ Rb/ ⁸⁶ Sr	⁸⁷ Sr/ ⁸⁶ Sr	±	Sr _i * 156 Ma	1/Sr	δ ¹⁸ O†	% yield
Uncles Creek pluton											
EP-141	tonalite	58.54	20.7	534	0.112	0.704073	0.000023	0.70382	0.00187	7.7	99.4
Heiney Bar pluton											
EP-289	granodiorite	69.40	71.1	353	0.583	0.705260	0.000011	0.70397	0.00283	9.5	95.4
English Peak pluton, early stage											
EP-23	tonalite	58.78	67.0	421	0.460	0.705314	0.000018	0.70429	0.00238	8.2	98.6
EP-54	Qz diorite	55.96	36.3	512	0.205	0.704811	0.000016	0.70436	0.00195	9.7	88.4
EP-94A	Qz monzodiorite	58.91	74.3	428	0.502	0.705391	0.000007	0.70428	0.00234	9.0	97.4
English Peak pluton, late stage											
<i>Border unit</i>											
EP-121	tonalite	60.21	50.8	435	0.338	0.705283	0.000012	0.70453	0.00230	9.5	100.1
EP-209A	granodiorite	61.20	58.9	412	0.414	0.705485	0.000012	0.70457	0.00243	9.4	100.7
<i>Yellow Jacket Ridge unit</i>											
EP-176B	Qz monzodiorite	52.52	72.8	457	0.461	0.705523	0.000014	0.70450	0.00219	9.0	98.8
<i>Chimney Rock unit</i>											
EP-163	granite	69.80	98.6	294	0.970	0.706760	0.000012	0.70461	0.00340	10.4	98.4
<i>Dikes</i>											
EP-78A	basalt	52.30	41.4	413	0.290	0.706211	0.000012	0.70557	0.00242	n.d.	n.d.
EP-80	basalt	52.96	35.6	488	0.211	0.705181	0.000011	0.70471	0.00205	n.d.	n.d.
EP-151	basalt	54.44	30.3	386	0.227	0.704858	0.000011	0.70435	0.00259	n.d.	n.d.
EP-210	Qz diorite	60.15	49.3	441	0.323	0.705146		0.70443	0.00227	n.d.	n.d.
<i>Mafic enclaves</i>											
EP-116	Qz diorite	52.00	27.0	527	0.148	0.704803	0.000056	0.70447	0.00190	n.d.	n.d.
EP-181A	diorite	50.24	77.9	645	0.349	0.705293	0.000010	0.70452	0.00155	n.d.	n.d.
Eastern Hayfork terrane host rocks											
EP-150D	argillite	42.07	163	192	2.458	0.714842	0.000012	0.71484	0.00521	13.9	95.3
EP-211B	phyllite	52.06	54.5	224	0.704	0.708856	0.000015	0.70886	0.00446	13.4	99.6
EP-213A	argillite	45.22	82.1	269	0.883	0.709853	0.000020	0.70985	0.00372	13.4	101.4

*Initial ⁸⁷Sr/⁸⁶Sr at 156 Ma.

†Per mil (V-SMOW).

n.d., not determined. Analysts: R. W. Kistler (Sr isotopes); H. R. Karlsson (oxygen isotopes).

of initial ⁸⁷Sr/⁸⁶Sr and δ¹⁸O values in the English Peak pluton are comparable with those characterizing other Wooley Creek suite plutons, suggesting a similar stage of deep-crustal magma evolution.

By analogy with other Wooley Creek suite plutons, we suggest that initiation of the Heiney Bar and then of the main English Peak pluton magmatism involved emplacement of basaltic magmas into the lower crust, initiating the development of a zone of mixing, assimilation, storage, and homogenization (MASH zone; Hildreth & Moorbath, 1988), in which metasedimentary rocks underwent partial melting, leading to hybridization of basaltic magmas with crust-derived magmas (Fig. 14). This MASH processing formed a range of mafic to intermediate magmas that gave rise first to the Heiney Bar pluton and then to the early stage of the English Peak pluton. These magmas varied in H₂O content and in Mg/(Mg + Fe_T), TiO₂, Al₂O₃, and many trace elements. Inasmuch as scant evidence supports significant differentiation of early stage magmas at the present level of emplacement, the compositional diversity of the unit must have developed deeper in the crust.

The higher initial ⁸⁷Sr/⁸⁶Sr and δ¹⁸O of late-stage rocks compared with early stage analogues suggests

that the younger magmas underwent greater degrees of contamination in the deep crust prior to upward transport. We envision formation of broadly andesitic magmas in the MASH zone and that these magmas rose to middle crustal levels (c. 15–20 km) where hornblende and plagioclase crystallized. The presence of diverse magmatic enclaves in the late stage suggests that mafic magmas probably also entered these mid-crustal reservoir(s), followed by mingling and mixing (Fig. 14; Schmidt, 1994). The mid-crustal magmas were episodically tapped, and rose into the shallow crust to form the late-stage units.

Similar major element compositions of hornblende core zones from all three late-stage units indicate that magmas for each unit ascended from the mid-crustal reservoir. Although we conclude that the border unit is not related to the interior units solely by fractional crystallization, it is possible that fractional crystallization combined with magma mixing explains the observed trace element changes in bulk-rock and hornblende compositions from the border unit to the Yellow Jacket Ridge and Chimney Rock units (Fig. 7e and f).

Decompression during final emplacement of late-stage magmas into the shallow crust (c. 7–10 km) resulted in partial resorption of olive-brown

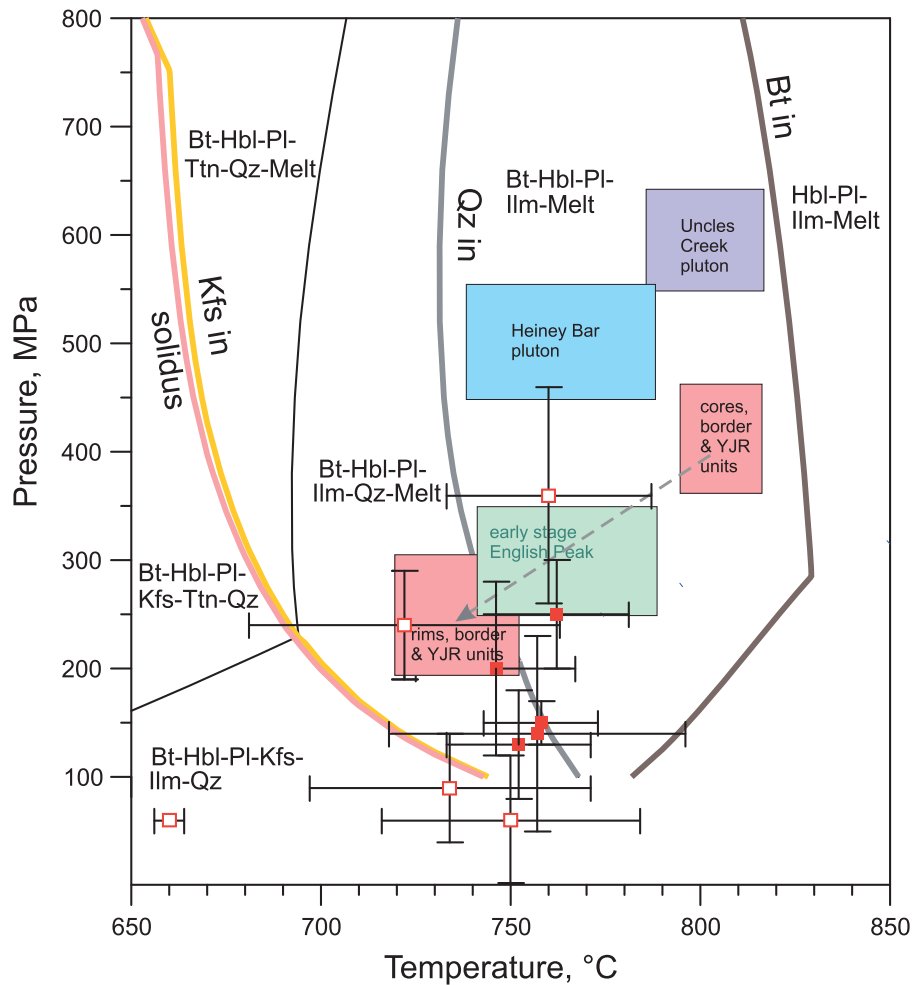


Fig. 13. Computed P - T conditions for granodiorite sample EP-216 from the Yellow Jacket Ridge unit. Square symbols represent P - T calculations according to Anderson & Smith (1995); filled red squares are for early stage samples, unfilled squares are late-stage samples. The larger boxes represent estimated P - T ranges using the Al-in-hornblende barometer of Schmidt (1992) and the hornblende thermometer of Putirka (2016). The size of the box represents the propagated uncertainty of means for each unit, with the exception of the box for the Heiney Bar pluton, which simply indicates the range of P - T estimates. The pink boxes represent P - T conditions estimated from core and rim compositions of hornblende from the border and Yellow Jacket Ridge (YJR) units of the late stage of the English Peak pluton. The unlabeled black curve represents the boundary between ilmenite stability at higher T and titanite stability. Mineral abbreviations after Whitney & Evans (2010).

hornblende, followed by growth of green hornblende rims. The remarkably large range of Ba contents in the border and Yellow Jacket Ridge units strongly suggests that after emplacement, melt percolation through a crystal-rich mush, prior to K-feldspar crystallization, was responsible for variable enrichment of bulk-rock Ba contents.

CONCLUSIONS

The English Peak plutonic complex illustrates the compositional diversity of magma types possible in retro-arc settings and in the transition from arc to retro-arc settings. This diversity is particularly evident in the early plutonic units, and reflects a change in crustal architecture following Uncles Creek magmatism and deep crustal injection of both Mg- and Fe-rich basalts

with variable H_2O contents during the onset of Heiney Bar and English Peak pluton magmatism. Magma evolution in a lower crustal MASH zone initially enhanced these compositional variations (Heiney Bar and early stage of the English Peak pluton). However, as this MASH zone matured, magmas that reached the middle and upper crust were restricted in bulk composition, presumably owing to the greater potential for homogenization in the MASH zone. Nevertheless, some mafic magmas were able to penetrate or bypass the MASH zone, leading to mixing and mingling in the mid-crustal reservoir, and potentially triggering upward mobility of magma into the upper crust. Our reconstruction of the EPC magma system indicates that it encompassed much of the crustal column but strongly suggests that lithological or tectonic boundaries in the crustal section led to magma ponding and consequent differentiation

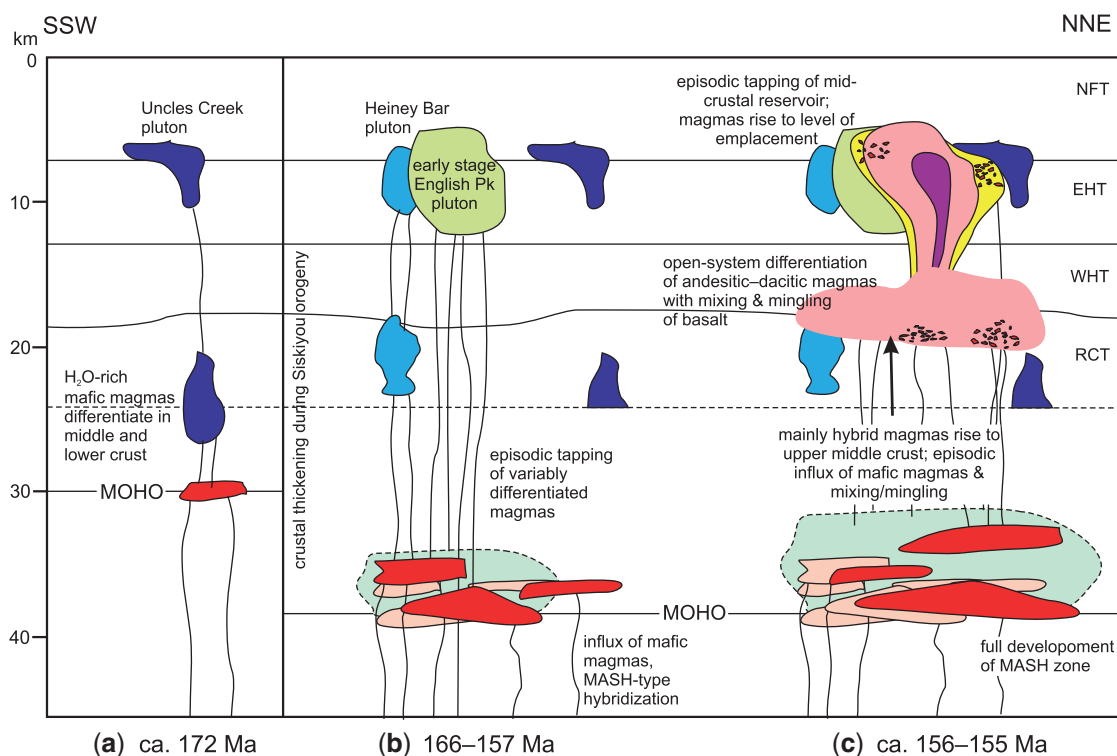


Fig. 14. Development of the English Peak plutonic complex through time. (a) Uncles Creek magmatism occurred in relatively thin crust prior to the Middle Jurassic Siskiyou orogeny and involved lower to middle crustal differentiation of H_2O -rich magmas. (b) Magmatism after the Siskiyou orogeny took place in thickened crust. Initial Heiney Bar activity resulted in ponding of magmas just above the Moho, followed by formation of magma chambers in the middle crust and then by emplacement in the upper crust. Continued influx of mafic magmas into the lower crust resulted in a MASH zone in which mafic magmas hybridized with lower crustal rocks and magmas. These hybrids rose episodically to form the early stage of the English Peak pluton. (c) Full development of the lower crustal MASH zone gives rise to magmas that rose to a middle-crustal reservoir, where olive-brown hornblende cores crystallized and localized magma mixing occurred. Progressively evolved magma from the mid-crustal reservoir rose to the upper crust to form the late stage of the English Peak pluton. Depth to the Moho in (a) is an estimate based on regional geological reconstructions (e.g. Snoke & Barnes, 2006). Post-Siskiyou Moho depth is from Barnes & Allen (2006), and depth to terrane boundaries is determined by projection from outcrop patterns. NFT, North Fork terrane; EHT, Eastern Hayfork terrane; WHT, Western Hayfork terrane; RCT, Rattlesnake Creek terrane. MASH, mixing, assimilation, storage, and homogenization.

(e.g. Hogan *et al.*, 1998). This reconstruction is distinct from both the hot zone model (Annen *et al.*, 2006) and models for plutonic systems in the Sierra Nevada batholith (e.g. Saleeby *et al.*, 2003; Paterson *et al.*, 2011) in which magma mush columns may extend from the Moho to the upper crust.

FUNDING

Our initial field research was part of a US Geological Survey wilderness resource evaluation project (Donato *et al.*, 1982). Partial support was also provided by NSF grants EAR-8720141 and EAR-9117103 to C.G.B.

SUPPLEMENTARY DATA

Supplementary data for this paper are available at *Journal of Petrology* online.

ACKNOWLEDGEMENTS

In addition to our work, results reported here utilized the detailed mapping, sampling, and petrographic

descriptions in PhD dissertations by Seyfert (1965) and Schmidt (1994). We thank Melanie Barnes, Ken Johnson, and Katie Gates for assistance in the field, and David Atwood for logistical support. We also thank M. Barnes and George Morgan for their able assistance in the laboratory. The paper was improved by helpful reviews from John Hogan, Lily Claiborne, and Diane Clemens-Knott, comments from Editor Jim Beard, and reviews of an early version of the paper from Nolwenn Coint and Charlotte Allen.

REFERENCES

- Allen, C. M. & Barnes, C. G. (2006). Ages and some cryptic sources of Mesozoic plutonic rocks in the Klamath Mountains, California. In: Snoke, A. W. & Barnes, C. G. (eds) *Geological Studies in the Klamath Mountains Province, California and Oregon: A volume in Honor of William P. Irwin*. Geological Society of America, *Special Papers* **410**, 223–245.
- Allen, J. C. & Boettcher, A. L. (1978). Amphiboles in andesite and basalt: II. Stability as a function of P - T - fH_2O - fO_2 . *American Mineralogist* **63**, 1074–1087.

- Allen, J. C. & Boettcher, A. L. (1983). The stability of amphibole in andesite and basalt at high pressures. *American Mineralogist* **68**, 307–314.
- Anderson, J. L. & Smith, D. R. (1995). The effects of temperature and fO_2 on the Al-in-hornblende barometer. *American Mineralogist* **80**, 549–559.
- Ando, C. J., Irwin, W. P., Jones, D. L. & Saleeby, J. B. (1983). The ophiolitic North Fork terrane in the Salmon River region, central Klamath Mountains, California. *Geological Society of America Bulletin* **94**, 236–252.
- Annen, C., Blundy, J. D. & Sparks, R. S. J. (2006). The genesis of intermediate and silicic magmas in deep crustal hot zones. *Journal of Petrology* **47**, 505–539.
- Barnes, C. G. (1983). Petrology and upward zonation of the Wooley Creek batholith, Klamath Mountains, California. *Journal of Petrology* **24**, 495–537.
- Barnes, C. G. & Allen, C. M. (2006). Depth of origin of late Middle Jurassic garnet andesite, southern Klamath Mountains. In: Snoke, A. W. & Barnes, C. G. (eds) *Geological Studies in the Klamath Mountains Province, California and Oregon: A Volume in Honor of William P. Irwin. Geological Society of America, Special Papers* **410**, 269–286.
- Barnes, C. G. & Barnes, M. A. (2013). The western Hayfork terrane: Middle Jurassic arc with adakitic affinities in the Klamath Mountain Province, OR and CA. *Geological Society of America, Abstracts with Programs* **45(6)**, 20.
- Barnes, C. G., Rice, J. M. & Gribble, R. F. (1986). Tilted plutons in the Klamath Mountains of California and Oregon. *Journal of Geophysical Research* **91**, 6059–6071.
- Barnes, C. G., Allen, C. M., Hoover, J. D., & Brigham, R. H. (1990). Magmatic components of a tilted plutonic system, Klamath Mountains, California. In: Anderson, J. L. (ed.) *The Nature and Origin of Cordilleran magmatism. Geological Society of America Memoir* **174**, 331–346.
- Barnes, C. G., Peterson, S. W., Kistler, R. W., Prestvik, T. & Sundvoll, B. (1992). Tectonic implications of isotopic variation among Jurassic and Early Cretaceous plutons, Klamath Mountains. *Geological Society of America Bulletin* **104**, 117–126.
- Barnes, C. G., Peterson, S. W., Kistler, R. W., Murray, R. & Kays, M. A. (1996). Source and tectonic implications of tonalite-trondhjemite magmatism in the Klamath Mountains. *Contributions to Mineralogy and Petrology* **124**, 40–60.
- Barnes, C. A., Mars, E. V., Swapp, S. & Frost, C. D. (2006). Petrology and geochemistry of the Middle Jurassic Ironside Mountain batholith: Evolution of potassic magmas in a primitive arc setting. In Snoke, A. W. & Barnes, C. G. (eds) *Geological Studies in the Klamath Mountains Province, California and Oregon: A Volume in Honor of William P. Irwin. Geological Society of America, Special Papers* **410**, 199–221.
- Bateman, P. C. & Chappell, B. W. (1979). Crystallization, fractionation, and solidification of the Tuolumne Intrusive Series, Yosemite National Park, California. *Geological Society of America Bulletin* **90(Part I)**, 465–482.
- Berry, R. A. (2015). Hornblende as an indicator of magma batches and magmatic processes in the English Peak pluton, Klamath Mountains, California. MS thesis, Texas Tech University, Lubbock, 201 pp.
- Boehnke, P., Watson, E. B., Trail, D., Harrison, T. M. & Schmitt, A. K. (2013). Zircon saturation re-revisited. *Chemical Geology* **351**, 324–334.
- Boynton, W. V. (1984). Cosmochemistry of the rare earth elements: meteorite studies. In: Henderson, P. (ed.) *Rare Earth Element Geochemistry. Developments in Geochemistry* **2**. Amsterdam: Elsevier, pp. 63–114.
- Coint, N., Barnes, C. G., Yoshinobu, A. S., Barnes, M. A. & Buck, S. (2013a). Use of trace element abundances in augite and hornblende to determine the size, connectivity, timing, and evolution of magma batches in a tilted pluton. *Geosphere* **9**, 1747–1765.
- Coint, N., Barnes, C. G., Yoshinobu, A. S., Chamberlain, K. R. & Barnes, M. A. (2013b). Batch-wise assembly and zoning of a tilted calc-alkaline batholith: Field relations, timing, and compositional variation. *Geosphere* **9**, 1729–1746.
- Coleman, R. G., Mortimer, N., Donato, M. M., Manning, C. E. & Hill, L. B. (1988). Tectonic and regional metamorphic framework of the Klamath Mountains and adjacent Coast Ranges, California and Oregon. In: Ernst, W. G. (ed.) *Metamorphism and Crustal Evolution of the Western United States*. Englewood Cliffs, NJ: Prentice-Hall, pp. 1061–1097.
- DeBari, S. & Coleman, R. (1989). Examination of the deep levels of an island arc: Evidence from the Tonsina ultramafic-mafic assemblage, Tonsina, Alaska. *Journal of Geophysical Research* **94**, 4373–4391.
- De Capitani, C. & Petrakakis, K. (2010). The computation of equilibrium assemblage diagrams with Theriak/Domino software. *American Mineralogist* **95**, 1006–1016.
- Donato, M. M. (1987). Evolution of an ophiolitic tectonic mélange, Marble Mountains, northern California Klamath Mountains. *Geological Society of America Bulletin* **98**, 448–464.
- Donato, M. M. (1989). Metamorphism of an ophiolitic tectonic mélange, northern California Klamath Mountains, U.S.A. *Journal of Metamorphic Geology* **7**, 515–528.
- Donato, M. M., Barnes, C. G., Coleman, R. G., Ernst, W. G. & Kays, M. A. (1982). Geologic map of the Marble Mountains Wilderness, Siskiyou County, California. *US Geological Survey, Miscellaneous Investigations Map MF-1452*, 1:48000.
- Donato, M. M., Barnes, C. G. & Tomlinson, S. L. (1996). The enigmatic Applegate Group of southwestern Oregon: Age, correlation, and tectonic affinity. *Oregon Geology* **58**, 79–91.
- Dorais, M. J. (1983). The geology and petrology of the Shelly Lake pluton, central Klamath Mountains, California. MS thesis, Eugene, University of Oregon, 147 pp.
- Droop, G. T. R. (1987). A general equation for estimating Fe^{3+} concentrations in ferromagnesian silicates and oxides from microprobe analyses, using stoichiometric criteria. *Mineralogical Magazine* **51**, 431–435.
- Eggler, D. H. (1972). Amphibole stability in H_2O -undersaturated calc-alkaline melts. *Earth and Planetary Science Letters* **15**, 28–34.
- Ernst, W. G. (1987). Mafic meta-igneous arc rocks of apparent komatiitic affinities, Sawyers Bar area, central Klamath Mountains, northern California. In: Mysen, B. O. (ed.) *Magmatic Processes: Physico-chemical Principles. Geochemical Society Special Publication* **1**, 191–208.
- Ernst, W. G. (1993a). Chemically distinct mafic dike/sill sequences of contrasting age ranges, Sawyers Bar area, central Klamath Mountains, northern California. *Journal of Petrology* **34**, 63–75.
- Ernst, W. G. (1993b). Geology of the Pacheco Pass quadrangle, central California Coast Ranges. *Geological Society of America, Maps and Charts Series MCH078*, scale 1:24000, accompanying text 12 pp.
- Ernst, W. G. (1998). Geology of the Sawyers Bar area, Klamath Mountains, northern California. *California Division of Mines and Geology, Map Sheet* **47**, scale 1:48000, accompanying text 59 pp.
- Ernst, W. G. (1999). Mesozoic petrotectonic development of the Sawyers Bar suprasubduction-zone arc, central Klamath

- Mountains, northern California. *Geological Society of America Bulletin* **111**, 1217–1232.
- Ernst, W. G. & Kolodny, Y. (1997). Submarine and superimposed contact metamorphic oxygen isotopic exchange in an oceanic arc, Sawyers Bar area, central Klamath Mountains, California, USA. *Geochimica et Cosmochimica Acta* **61**, 821–834.
- Ernst, W. G. & Liu, J. (1998). Experimental phase-equilibrium study of Al- and Ti-contents of calcic amphibole in MORB—a semiquantitative thermobarometer. *American Mineralogist* **83**, 952–969.
- Ernst, W. G., Hacker, B. R., Barton, M. D. & Sen, G. (1991). Igneous petrogenesis of magnesian metavolcanic rocks from the central Klamath Mountains, northern California. *Geological Society of America Bulletin* **103**, 56–72.
- Frost, B. R., Barnes, C. G., Collins, W. J., Arculus, R. J., Ellis, D. J. & Frost, C. D. (2001). A geochemical classification for granitic rocks. *Journal of Petrology* **42**, 2033–2048.
- Garcia, M. O. (1979). Petrology of the Rogue and Galice formations, Klamath Mountains, Oregon: Identification of a Jurassic island arc sequence. *Journal of Geology* **87**, 29–41.
- Garcia, M. O. (1982). Petrology of the Rogue River island-arc complex, southwest Oregon. *American Journal of Science* **282**, 783–807.
- Garlick, S. R., Medaris, L. G., Jr, Snoko, A. W., Schwartz, J. J. & Swapp, S. M. (2009). Granulite- to amphibolite-facies metamorphism and penetrative deformation in a disrupted ophiolite, Klamath Mountains, California: A deep view into the basement of an accreted oceanic arc. In: Miller, R. B. & Snoko, A. W. (eds) *Crustal Cross Sections from the Western North American Cordillera and Elsewhere: Implications for Tectonic and Petrologic Processes*. Geological Society of America, *Special Papers* **456**, 151–186.
- Gates, K. (2015). A quantitative analysis of xenolith fragmentation and incorporation in magma. MS thesis, Texas Tech University, Lubbock, 210 pp.
- Goode, J. W. (1989). Polyphase metamorphic evolution of a Late Triassic subduction complex, Klamath Mountains, northern California. *American Journal of Science* **289**, 874–943.
- Goode, J. W. (1995). Pre-Middle Jurassic accretionary metamorphism in the southern Klamath Mountains of northern California. *Journal of Metamorphic Geology* **13**, 93–110.
- Greene, A. R., DeBari, S. M., Kelemen, P. B., Blusztajn, J. & Clift, P. D. (2006). A detailed geochemical study of island arc crust: the Talkeetna arc section, south-central Alaska. *Journal of Petrology* **47**, 1051–1093.
- Hacker, B. R., Ernst, W. G. & Barton, M. D. (1992). Metamorphism, geochemistry and origin of magnesian volcanic rocks, Klamath Mountains, California. *Journal of Metamorphic Geology* **10**, 55–69.
- Hacker, B. R., Ernst, W. G. & McWilliams, M. O. (1993). Genesis and evolution of a Permian–Jurassic magmatic arc/accretionary wedge, and reevaluation of terranes in the central Klamath Mountains. *Tectonics* **12**, 387–409.
- Hacker, B. R., Donato, M. M., Barnes, C. G., McWilliams, M. O. & Ernst, W. G. (1995). Timescales of orogeny: Jurassic construction of the Klamath Mountains. *Tectonics* **14**, 677–703.
- Harper, G. D. & Wright, J. E. (1984). Middle to Late Jurassic tectonic evolution of the Klamath Mountains, California–Oregon. *Tectonics* **3**, 759–772.
- Harper, G. D., Saleeby, J. B. & Heizler, M. (1994). Formation and emplacement of the Josephine ophiolite and the Nevadan orogen in the Klamath Mountains, California–Oregon: U/Pb zircon and $^{40}\text{Ar}/^{39}\text{Ar}$ geochronology. *Journal of Geophysical Research* **99**, 4293–4321.
- Hildreth, W. & Moorbath, S. (1988). Crustal contributions to arc magmatism in the Andes of central Chile. *Contributions to Mineralogy and Petrology* **98**, 455–489.
- Hogan, J. P., Price, J. D. & Gilbert, M. C. (1998). Magma traps and driving pressure: consequences for pluton shape and emplacement in an extensional regime. *Journal of Structural Geology* **20**, 1155–1168.
- Holland, T. J. B. & Blundy, J. (1994). Non-ideal interactions in calcic amphiboles and their bearing on amphibole–plagioclase thermometry. *Contributions to Mineralogy and Petrology* **116**, 433–447.
- Holland, T. J. B. & Powell, R. (1998). An internally consistent thermodynamic data set for phases of petrological interest. *Journal of Metamorphic Geology* **16**, 309–343.
- Hotz, P. E., (1971). Plutonic rocks of the Klamath Mountains, California and Oregon. *U.S. Geological Survey Professional Paper* **684-B**, 1–20.
- Hotz, P. E., Lanphere, M. A. & Swanson, D. A. (1977). Triassic blueschist from northern California and north-central Oregon. *Geology* **5**, 659–663.
- Irwin, W. P. (1960). *Geologic reconnaissance of the northern Coast Ranges and the southern Klamath Mountains, California, with a summary of the mineral resources*. California Division of Mines Bulletin **179**, 80 pp.
- Irwin, W. P. (1972). Terranes of the western Paleozoic and Triassic belt in the southern Klamath Mountains, California. *US Geological Survey, Professional Papers* **800-C**, C103–C111.
- Irwin, W. P. (1981). Tectonic accretion of the Klamath Mountains. In: Ernst, W. G. (ed.) *The Geotectonic Development of California*. Englewood Cliffs, NJ: Prentice-Hall, pp. 29–49.
- Irwin, W. P. (1985). Age and tectonics of plutonic belts in accreted terranes of the Klamath Mountains, California and Oregon. In: Howell, D. G. (ed.) *Tectonostratigraphic Terranes of the Circum-Pacific Region*. Circum-Pacific Council for Energy and Mineral Resources; *Earth Science Series* **1**, 187–199.
- Irwin, W. P. (1994). Geologic Map of the Klamath Mountains, California and Oregon. *US Geological Survey, Miscellaneous Investigations Series Map* **1-2148**, scale 1:500 000.
- Irwin, W. P. & Wooden, J. L. (1999). *Plutons and accretionary episodes of the Klamath Mountains, California and Oregon*. *US Geological Survey, Open-File Report* **99-374**.
- Jagoutz, O.E. (2010). Construction of the granitoid crust of an island arc. Part II: a quantitative petrogenetic model. *Contributions to Mineralogy and Petrology* **160**, 359–381.
- Jagoutz, O. E., Burg, J.-P., Hussain, S. S., Dawood, H., Pettke, T., Iizuka, T. & Maruyama, S. (2009). Construction of the granitoid crust of an island arc part I: geochronological and geochemical constraints from the plutonic Kohistan (NW Pakistan). *Contributions to Mineralogy and Petrology* **158**, 739–755.
- Lanphere, M. A., Irwin, W. P. & Hotz, P. E. (1968). Isotopic age of the Nevadan Orogeny and older plutonic and metamorphic events in the Klamath Mountains, California. *Geological Society of America Bulletin* **79**, 1027–1052.
- Leake, B., Woolley, A., Arps, C., Birch, W., Gilbert, M., Grice, J., Hawthorne, F., Kato, A., Kisch, H., Krivovichev, V., Linthout, K., Laird, J., Mandarino, J., Schumacher, J., Smith, D., Stephenson, N., Ungaretti, L., Whittaker, E. & Youzhi, G. (1997). Nomenclature of amphiboles: Report of the Subcommittee on Amphiboles of the International Mineralogical Association, Commission on New Minerals and Mineral Names. *American Mineralogist* **82**, 1019–1037.
- Mankinen, E. A., Irwin, W. P. & Blome, C. D. (1996). Far-travelled Permian chert of the North Fork terrane, Klamath Mountains, California. *Tectonics* **15**, 314–328.

- Medaris, L. G., Jr, Lapen, T. J., Jicha, B. R., Singer, B. S., Ghent, E. D. & Garlick, S. R. (2009). 168 Ma granulite facies metamorphism and 154 Ma refrigeration in the Seiad metaophiolite complex, Rattlesnake Creek terrane, Klamath Mountains. *Geological Society of America, Abstracts with Programs* **41**, 590.
- Naney, M. T. (1983). Phase equilibria of rock-forming ferromagnesian silicates in granitic systems. *American Journal of Science* **283**, 993–1033.
- Otamendi, J. E., Tibaldi, M. N., Bergantz, A. M., Bergantz, G. W., De La Rosa J. D., & Vujovich, G. I. (2009). Generation of tonalitic and dioritic magmas by coupled partial melting of gabbroic and metasedimentary rocks within the deep crust of the Famatinian magmatic arc, Argentina. *Journal of Petrology* **50**, 841–873.
- Otamendi, J. E., Ducea, M. N. & Bergantz, G. W. (2012). Geological, petrological and geochemical evidence for progressive construction of an arc crustal section, Sierra de Valle Fértil, Famatinian arc, Argentina. *Journal of Petrology* **53**, 761–800.
- Paterson, S. R., Okaya, D., Memeti, V., Economos, R. & Miller, R. B. (2011). Magma addition and flux calculations of incrementally constructed magma chambers in continental margin arcs: Combined field, geochronologic, and thermal modeling studies. *Geosphere* **7**, 1439–1468.
- Putirka, K. (2008). Thermometers and barometers for volcanic systems. In: Putirka, K. & Tepley, F. J., III (eds) *Minerals, Inclusions and Volcanic Processes. Mineralogical Society of America and Geochemical Society, Reviews in Mineralogy and Geochemistry* **69**, 61–120.
- Putirka, K. (2016). Amphibole thermometers and barometers for igneous systems, and some implications for eruption mechanisms of felsic magmas at arc volcanoes. *American Mineralogist*, **101**, 841–858.
- Saleeby, J., Ducea, M. & Clemens-Knott, D. (2003). Production and loss of high-density batholithic root, southern Sierra Nevada, California. *Tectonics* **22**, doi:10.1029/2002TC001374.
- Scherer, H. H. & Ernst, W. G. (2008). North Fork terrane, Klamath Mountains, California: Geologic, geochemical, and geochronologic evidence for an early Mesozoic forearc. In: Wright, J. E. & Shervais, J. W. (eds) *Ophiolites, Arcs, and Batholiths: A Tribute to Cliff Hopson. Geological Society of America, Special Papers* **438**, 289–309.
- Scherer, H. H., Ernst, W. G. & Wooden, J. L. (2010). Regional detrital zircon provenance of exotic metasandstone blocks, Eastern Hayfork terrane, Western Paleozoic and Triassic belt, Klamath Mountains, California. *Journal of Geology* **118**, 641–653.
- Schmidt, B. L. (1994). The petrology and geochemistry of the English Peak intrusive suite, Klamath Mountains, California. PhD dissertation, Texas Tech University, Lubbock, 216 pp.
- Schmidt, M. W. (1992). Amphibole composition in tonalite as a function of pressure: an experimental calibration of the Al-in-hornblende barometer. *Contributions to Mineralogy and Petrology* **110**, 304–310.
- Seyfert, C., Jr (1965). Geology of the Sawyers Bar area, Klamath Mountains, northern California. PhD dissertation, Stanford University, Stanford, CA, 227 pp.
- Snoko, A. W. & Barnes, C. G. (2006). The development of tectonic concepts for the Klamath Mountains province, California and Oregon. In: Snoko, A.W. & Barnes, C.G. (eds) *Geological studies in the Klamath Mountains province, California and Oregon: A volume in honor of William P. Irwin. Geological Society of America Special Paper* **410**, 1–29.
- Whitney, D. L. & Evans, B. W. (2010). Abbreviations for names of rock-forming minerals. *American Mineralogist* **95**, 185–187.
- Wright, J. E. (1982). Permo-Triassic accretionary subduction complex, southwestern Klamath Mountains, northern California. *Journal of Geophysical Research* **87**, 3805–3818.
- Wright, J. E. & Fahan, M. R. (1988). An expanded view of Jurassic orogenesis in the western United States Cordillera: Middle Jurassic (pre-Nevadan) regional metamorphism and thrust faulting within an active arc environment, Klamath Mountains, California. *Geological Society of America Bulletin* **100**, 859–876.
- Wright, J. E. & Wyld, S. J. (1994). The Rattlesnake Creek terrane, Klamath Mountains, California: An early Mesozoic volcanic arc and its basement of tectonically disrupted oceanic crust. *Geological Society of America Bulletin* **106**, 1033–1056.